Article:
Doherty, CPA orcid.org/0000-0001-5685-4716, Young, LM, Karamanos, TK et al. (4 more authors) (2018) A peptide-display protein scaffold to facilitate single molecule force studies of aggregation-prone peptides. Protein Science, 27 (7). pp. 1205-1217. ISSN 0961-8368

https://doi.org/10.1002/pro.3386

A peptide-display protein scaffold to facilitate single molecule force studies of aggregation-prone peptides

Authors:

Ciaran P A Doherty[1, 2], Lydia M Young[1,2], Theodoros K Karamanos[1,2], Hugh I Smith[1,2], Matthew P Jackson[1,2], Sheena E Radford[1, 2], David J Brockwell[1, 2]

Affiliations:

[1] Astbury Centre for Structural Molecular Biology, University of Leeds, LS2 9JT, United Kingdom

[2] School of Molecular and Cellular Biology, Faculty of Biological Sciences, University of Leeds, LS2 9JT, United Kingdom

Corresponding author:

David J Brockwell

0113 343 7821

D.J.Brockwell@leeds.ac.uk

Running Title:

Developing a peptide display system for force spectroscopy

Abstract

Protein aggregation is linked with the onset of several neurodegenerative disorders, including Parkinson's disease (PD), which is associated with the aggregation of α-synuclein (αSyn). The structural mechanistic details of protein aggregation, including the nature of the earliest protein:protein interactions, remain elusive. In this study we have used single molecule force spectroscopy (SMFS) to probe the first dimerisation events of the central aggregation-prone region of αSyn (residues 71-82) that may initiate aggregation. This region has been shown to be necessary for the aggregation of full length αSyn and is capable of forming amyloid fibrils in isolation. We demonstrate that the interaction of αSyn_{71-82} peptides can be studied using SMFS when inserted into a loop of protein L, a mechanically strong and soluble scaffold protein that acts as a display system for SMFS studies. The corresponding fragment of the homologous protein γ-synuclein (γSyn), which has a lower aggregation propensity, has also been studied here. The results from SMFS, together with native mass spectrometry and aggregation assays, demonstrate that the dimerisation propensity of γSyn_{71-82} is lower than that of αSyn_{71-82}, but that a mixed αSyn_{71-82}: γSyn_{71-82} dimer forms with a similar propensity to the αSyn_{71-82} homodimer, slowing amyloid formation. This work demonstrates the utility of a novel display method for SMFS studies of aggregation-prone peptides which would otherwise be difficult to study.

Impact statement

In this study, a display system for the investigation of the intermolecular interactions of small, aggregation-prone peptides via SMFS has been developed and validated. The data obtained using this method provides insight on the interactions between the central aggregation-prone region of αSyn and its homologue γSyn, revealing an inhibitory interaction of γSyn on αSyn aggregation by formation of heterodimers.

Key words

Single molecule force spectroscopy, alpha-synuclein, gamma-synuclein, aggregation, amyloid, mass spectrometry

Introduction

Studying protein aggregation is a significant challenge, owing to the fact that the aggregating species along the assembly pathway are often heterogeneous, transiently populated and evolve on an exponential timescale towards higher order, end point species(1-3). Early events in the aggregation cascade are consequently difficult to study but are of critical importance in enhancing our fundamental understanding of the aggregation process. Gaining a greater mechanistic and structural understanding of early events in aggregation is especially important for amyloid diseases where the identity of the toxic species is still unclear(4). Inhibition of early events in the aggregation cascade are thus attractive targets for preventative and curative treatments for these diseases.

Single molecule approaches using fluorescence(5; 6), or force spectroscopy using either the AFM(7-17) or optical tweezers(18) are potentially powerful methods to interrogate aggregating systems as they can be performed at low concentrations, limiting aggregation and decreasing the rate of assembly. In SMFS, monomers of the aggregation-prone species are immobilised to force sensors, separating the first protein-protein interactions from heterogeneous higher order species that complicate data analysis in other approaches. SMFS can yield information on both the strength of the interaction (and therefore off rates)(19) and on the location of the interaction interface via measurement of the end-to-end length of the complex at rupture(20). Application of SMFS to the aggregation field, however, is challenging due to difficulties in deconvoluting non-specific interactions from *bone fide* protein-protein interactions, both of which usually occur close to the surface (21). Separation of signal from noise is especially challenging when studying small aggregation-prone proteins, such as Aβ42(22), or peptide fragments from larger proteins that are thought to drive aggregation

such as the non-amyloid component (NAC) region of αSyn (23; 24). This is because these peptides can interact with inert surfaces and take part in multipartite interactions between the tip and surface. As the peptide end-to-end length is inherently short (<5 nm), these non-specific interactions occur close to the surface. For experiments that extend a single protein (mechanical unfolding), some of these problems have been addressed by site-specific immobilisation onto passivated surfaces(25) or by insertion of the protein of interest into a mechanically strong protein within a protein concatemer(26). For protein-protein interaction studies, Lyubchenko and colleagues have developed a "flexible nanoarray" method(27; 28) whereby pairs of aggregation-prone peptides are tethered onto an extensible linker at a defined separation, allowing dimerisation events to be analysed(27). Extending the tether using the AFM allows dissociation to be measured away from the surface. While allowing measurement of dissociation, this approach requires the synthesis of bespoke polyethylene glycol-phosphoramidite linkers(21). Another approach developed by Carrion-Vasquez and colleagues(29) used a disulphide-linked polyprotein construct that allowed direct identification of single molecule dissociation events of the highly avid cohesin–dockerin complex. This method allows for internally controlled SMFS experiments on protein-protein interactions. It is, however, complex to implement, requires formation of a trimer and has not been used to analyse intermolecular interactions in a non-cognate, aggregation-prone system.

In this study, we report the development and validation of a novel, easy to implement method in which an aggregation-prone region of a protein of interest is engineered into a loop of the mechanically stable monomeric carrier protein, protein L. The central NAC region (residues 71-82) of αSyn (part of the wider NAC region encompassing residues 61-95) was chosen to

assess this display system as this hydrophobic, 12-residue sequence (^{71}VTGVTAVAQKT^{82}V) is known to be both sufficient and necessary for aggregation(24) and to form the core of fibrils of wild-type αSyn (30). We show that protein L is a suitable scaffold protein, maintaining its structure and stability after insertion of guest sequences. SMFS experiments using an AFM tip and surface derivatised with the protein L scaffold containing αSyn_{71-82} yield rupture events with correlated dissociation force and unfolding distances. By contrast, protein L constructs containing a control $(GS)_6$ linker or γSyn_{71-82} (the central NAC region derived from the less aggregation-prone γSyn homologue of αSyn(31; 32)) yielded insignificant rupture events. Interestingly, an interaction is observed between αSyn_{71-82} and γSyn_{71-82} using SMFS in the pL scaffold, consistent with the postulated interaction between the full length proteins(32). We then use native electrospray ionisation-ion mobility spectrometry-mass spectrometry (ESI-IMS-MS), which enables the detailed interrogation of individual species within a heterogeneous, assembling mixture(33-37), to validate these results. SMFS can thus yield novel insight into the early stages of amyloid formation by insertion of aggregation-prone sequences of interest into the mechanically and thermodynamically stable scaffold, protein L.

Results

Design and characterisation of a protein L scaffold.

A scaffold protein should (a) allow the presentation of the amyloidogenic peptide in a defined geometry away from the surface; (b) be thermodynamically and mechanically stable after insertion of the sequence of interest and (c) display minimal self aggregation. The IgG binding domain of protein L (Figure 1A) fulfils these criteria. This protein comprises a four stranded β-sheet packed against an α-helix and has been shown previously to withstand the insertion of both folded and unfolded amino-acid sequences into the β3-β4 loop(38) and to show mechanical resistance when extended via its termini(39). The scaffold shown in Figure 1A is based on protein L W47Y I60F (herein termed pL), a variant rationally designed to display enhanced mechanical strength(40). To ensure that the guest peptide sequence is sterically free from the pL host, the amyloidogenic peptide was inserted into the centre of the β3-β4 loop that had been extended by 13 residues (generating ^{55}G…GGARGS…guest peptide…GSARGGG…^{56}Y, Supplementary Figure S1). Finally, a cysteine residue was introduced into the β1-β2 loop (N14C) distal to the graft site. This allows the specific immobilisation of the scaffold onto a substrate in a geometry that presents the guest sequence to the solution (allowing dimerisation when immobilised onto the AFM tip and surface, Figure 1B) and that upon extension would shear the pL N- and C-terminal strands apart. This extension geometry has previously been shown to be mechanically robust(39; 40).

pL scaffolds presenting αSyn$_{71-82}$ (Supplementary Figure S2) and a twelve-residue non-aggregating control sequence ((GS)$_6$, herein named GS) were constructed and each protein expressed and purified (Supplementary Figure S3, Materials and Methods). After verification of protein identity by ESI-MS (Supplementary Table 1), the structural integrity of each

construct was assessed by far-UV CD and fluorescence emission spectroscopy. These experiments verified that all three proteins exhibited CD-spectra consistent with a mixed α/β topology similar to that reported for wild-type protein L(41) (Supplementary Figure S4A). Similarly, fluorescence emission spectra which exhibit a red shift in their maxima upon denaturant-induced unfolding were observed for all proteins (Supplementary Figure S4B). As expected for natively folded variants of protein L, thermal denaturation monitored by far-UV CD revealed co-operative unfolding transitions at a similar temperature for pL GS and pL αSyn_{71-82} (T_m values of 45.5 and 46.6 ^oC, respectively, Supplementary Figures S4C and D).

As a more sensitive probe for structural perturbations, the ^1H-^{15}N heteronuclear single quantum coherence spectroscopy (HSQC) NMR spectra of pL αSyn_{71-82} and pL GS were acquired (Figure 2). Both spectra show similarly dispersed, well defined peaks of similar intensity, characteristic of stably folded proteins (Figure 2A). Five additional main chain peaks were observed for pL αSyn_{71-82} compared with pL GS (Figure 2B), likely due to the chemical shift redundancy of the glycine residues in the $(GS)_6$ linker and extended loop. Most of the additional peaks for pL αSyn_{71-82} are observed at ^1H chemical shifts that are diagnostic of an unfolded protein conformation (~8.0 ppm), suggesting that these peaks indeed arise from the αSyn_{71-82} in an unfolded conformation within the loop region. Overall, the CD, fluorescence and NMR data show that grafting a twelve residue peptide sequence into the extended β3-β4 loop does not perturb the structure or stability of pL, validating its use a display scaffold for SMFS experiments.

Dimerisation of the αSyn central NAC region detected by SMFS

To determine whether the association of αSyn_{71-82} could be detected in the context of the protein L scaffold using AFM-based SMFS methods, the AFM probe and surface were each

decorated with either pL αSyn_{71-82} or pL GS (Materials and Methods). After mounting in the AFM, force-extension profiles were accumulated. After filtering (Materials and Methods), traces which showed a characteristic single molecule "saw tooth" profile (Figure 1C) were binned for analysis. The number of these events relative to the total number of approach-retract cycles (in triplicate) was then used to calculate a 'hit rate' which reports on the probability of measuring the rupture (and therefore the presence) of a protein-protein interaction. As shown in Figure 1C, for each force-extension profile, the force at rupture (F_R) of the interaction and the end-to-end length of the dimer (L_c) at rupture was measured. To obtain L_c, force-extension profiles were fitted to the WLC model (Materials and Methods, Equation 1). Finally, to assess whether the observed dissociation events produced reproducible and correlated values of L_C and F_R, contour plots were generated (Figure 3).

Comparison of the force-extension profiles and contour plots obtained for pL αSyn_{71-82} and pL GS (Figure 3A, B) revealed that the dissociation of pL αSyn_{71-82}, but not pL GS, can be detected and quantified using SMFS. Force-extension profiles for pL αSyn_{71-82} typically produced a single sawtooth (Figure 3A), as expected for an extensible chain(42) with correlated F_R and L_C values (57 ±1 pN and 22 ±1 nm, respectively) and a hit-rate of 4.0 ± 0.7 %. By contrast, force-extension profiles for pL GS were generally featureless (Figure 3B). For this protein, the frequency of binned events was lower (1.6 ± 0.2 %) with no 'hotspot' (diagnostic of a specific interaction) in the contour plot. These data indicate that SMFS can detect intermolecular interactions between amyloidogenic peptides. The modal rupture force is surprisingly large given the expected transient nature and the relatively small interaction surface of the 12-residue αSyn peptide (F_R = 57 pN, at a retraction velocity of 1000 nms^{-1}). F_R is similar, however,

to that measured for full length αSyn(14; 16; 17) and other protein:protein interactions mediated by short peptide sequences(43).

Dynamic force spectroscopy of the αSyn central NAC region

Despite the small size of the peptide fragment αSyn_{71-82} under study here, the data demonstrate that interaction between these sequences is sufficiently strong to be detected by SMFS. In order to characterise this dimer interaction further, Dynamic Force Spectroscopy (DFS) was carried out allowing parameters of the unbinding energy landscape to be calculated (Figure 4A). The SMFS experiments were carried out at pulling velocities ranging from 200 – 5000 nms^{-1} (Figure 4B). After calculation of the loading rate at rupture Materials and Methods, Equation 2), the dissociation rate constant in the absence of force (k_{off}^{0F}) and the 'distance' between the dissociation energy barrier and the bound ground state (x_u) was calculated using the Bell-Evans model(44; 45) (Materials and Methods, Equation 3). The dissociation rate constant for pLαSyn_{71-82} dimers (k_{off}^{0F} = 0.18 s^{-1}, lifetime ~ 6s) is comparable to the dissociation rate constant of full length αSyn (0.25 s^{-1} at pH 2.7 and 0.74 s^{-1} at pH 3.7 measured by SMFS)(9). The finding that the lifetimes of dimers of full length αSyn and αSyn_{71-82} dimers are of comparable magnitude suggests that residues 71-82 play a key role in the stability of dimeric species formed from the intact protein.

SMFS identifies a novel interaction between αSyn_{71-82} and its homologue γSyn_{71-82}

While the presence or absence of SMFS rupture peaks for dimers of pL αSyn_{71-82} and pL GS, respectively suggests that the former protein self-interacts, it does not report on the specificity of this interaction. To address this question, we inserted the central NAC domain of another member of the synuclein family, γSyn, into the pL scaffold. The central NAC sequences of α- and γ-Syn differ at five positions (αSyn: ^{71}VTGVTAVAQKTV$_{82}$ and γSyn:

$_{71}$VSSVNTVATKTV^{82}) and these differences (Supplementary Figure S2) may play a role in the greater amyloidogenic propensity observed for αSyn(31; 32).

After construction, purification and characterisation of pL γSyn$_{71-82}$ (Supplemental Figure S3 and S4, Supplementary Table 1), SMFS was used to probe homodimeric (pL γSyn$_{71-82}$ on the AFM tip and surface) and heterodimeric (pL γSyn$_{71-82}$ on the AFM tip and pL αSyn$_{71-82}$ on surface) dissociation events. Surprisingly, the force-extension profiles and contour plots for putative homodimeric pL γSyn$_{71-82}$ dissociation (Figure 5A) show no evidence for formation of a force-resistant structure (hit rate = 0.6 ± 0.3 %, no 'hot spot' evident). By contrast, the dissociation of pL γSyn$_{71-82}$:pL αSyn$_{71-82}$ heterodimers was readily detected using SMFS yielding comparable L_C and F_R values (19 ± 1 nm and 53 ± 1 pN, respectively) to that of the αSyn$_{71-82}$ homodimeric interaction, albeit at a lower frequency of detection (3.2 ± 0.8 %). Importantly, the possibility that these observations arise from differences in immobilisation efficiencies between each scaffold was ruled out by sequential experiments that used the same derivitised tip but different substrates (Supplemental Figure S5). The results thus portray the first observation of a heterodimeric interaction in an aggregating system by SMFS and also the first observation that the central NAC region of αSyn is sufficient to interact with the corresponding sequence of its homologue γSyn. Uversky and colleagues have shown previously that full length αSyn fibrillation is inhibited by the presence of γSyn(32). One possible interpretation is that this inhibitory effect is mediated by the interaction between the central NAC regions of these proteins.

Native mass spectrometry of pL constructs

SMFS shows that the central NAC regions of α- and γSyn are able to dimerise and be of sufficient kinetic stability to measure their dissociation using force spectroscopy. To verify this

observation, ESI-MS was used as an orthogonal method to detect dimerisation. This soft ionisation method enables preservation of non-covalent interactions in the gas phase and allows resolution of heterogeneous species that differ in mass or charge state and, when coupled to ion mobility spectrometry (ESI-IMS-MS), cross-sectional area (46). These experiments were performed using 100 µM pL constructs in 100 mM ammonium acetate pH 6.8 and, to measure formation of heterodimers, equal volumes of each sample were mixed. ESI-MS data were then accumulated immediately (t = 0) or after quiescent incubation for 4 h at 25 °C. Comparison of the ESI mass spectra for pL GS, pL αSyn_{71-82}, pL γSyn_{71-82} and 1:1 pL αSyn_{71-82}:pL γSyn_{71-82} showed that all pL constructs were initially monomeric upon dilution (t = 0, Supplemental Figure S6). In accord with the SMFS experiments described above, pL GS remained monomeric after incubation. In contrast, dimers, in addition to monomers, were observed for pL γSyn_{71-82} alone, with monomers-trimers present for pL αSyn_{71-82} and for mixtures of 1:1 pL αSyn_{71-82}:pL γSyn_{71-82} (Supplementary Figure S6). For each charge state of the heterodimeric species, the difference in the molecular masses of pL αSyn_{71-82} and pL γSyn_{71-82} (10,391 and 10,423 Da, respectively) is sufficient to resolve three peaks representing homodimers of pL αSyn_{71-82} and pL γSyn_{71-82} (at m/z values centred on ~2282 and 2289, Figure 6) and a heterodimer (m/z centred on ~2285) corroborating the observation of a heterodimer in SMFS experiments. Interestingly, despite mixing an equal concentration of each variant, the relative intensity of each dimer species differs and mirrors the hit rate observed by SMFS experiments (from highest to lowest apparent dimer population: $\alpha\alpha > \alpha\gamma > \gamma\gamma$). In the mixed samples, peaks from monomeric proteins (Supplementary Figure S6) were of similar intensities, suggesting that the two peptides ionise with similar efficiency. This observation suggests that the intensities of dimer peaks indeed reflect the relative affinity of the different dimeric species.

To preclude the possibility that the interactions observed by SMFS and ESI-MS arise from the pL scaffold, the ESI-MS experiments were repeated using αSyn_{71-82} and γSyn_{71-82} as synthetic peptides. ESI-IMS-MS driftscope plots of the peptides alone and in a 1:1 mixture showed the presence of monomeric to tetradecameric species (Supplemental Figure S7). The higher order of species observed for the peptide-only variants suggests that packing restraints of the scaffold disfavours larger oligomer formation. Despite these differences, homodimers and heterodimers were formed upon mixing equimolar αSyn_{71-82}:γSyn_{71-82}, confirming that αSyn_{71-82} and γSyn_{71-82} sequences interact independently of the pL scaffold.

Characterising the aggregation of pL constructs

We have shown that the central NAC regions of αSyn and γSyn are sufficient to allow the formation of transient homo- and hetero-dimers and that this interaction is preserved when these short sequences are inserted into the pL scaffold. To investigate whether these pL-peptide chimeras are able to form amyloid fibrils, we examined the amyloid growth kinetics of pL αSyn_{71-82} and pL γSyn_{71-82} using thioflavin T (ThT) fluorescence (Figure 7). In addition, as full length γSyn has previously been shown to inhibit the kinetics of αSyn aggregation(32), we also measured the amyloid growth kinetics of a 1:1 mixture of pL αSyn_{71-82} and pL γSyn_{71-82} to test whether this inhibitory interaction was mediated by the central NAC region. The end point of ThT fluorescence emission intensity was similar for both pL αSyn_{71-81} and pL γSyn_{71-82} (785 ± 122 and 929 ± 83 arbitrary units, respectively after 100 h) while the mixed sample appeared unable to aggregate as studied by this assay (Figure 7). pL GS did not aggregate into ThT-positive species. Similar experiments performed on the synthetic peptides also showed that a 1:1 mixture of αSyn_{71-81} and γSyn_{71-82} resulted in a significant increase in lag-time (2.5 x and 5.7 x increase when compared with αSyn_{71-82} and γSyn_{71-}82 alone, respectively

(Supplemental Figure S8)). These data suggest that the heterodimeric interaction identified by SMFS and ESI-MS inhibits aggregation. This supports the finding that the inhibitory effect reported for full length γSyn on the aggregation of αSyn is mediated by the interaction between their central NAC regions. It is important to note however, that the SMFS and ESI-MS experiments were carried out in different buffer conditions due to the buffer limitations in ESI-MS experiments. It is widely recognised that ionic strength and pH affect the rates and the dominating mechanisms in amyloid formation (47-49). However, the inhibitory effect that γSyn_{71-82} exerts on αSyn_{71-82} was also observed in aggregation assays performed in ESI- MS buffer conditions (Figure S9).

Discussion

In this study we describe the generation, characterisation and proof-of-concept of a novel approach to facilitate the investigation of interactions between amyloidogenic peptides using SMFS. Using protein L as a display system, we were able to interrogate the specific interactions between synuclein sequences and to minimise the contributions of non-specific events that often occur at the surface-proximal regions of force-distance curves(50). Our approach also restricts the application of force to a defined geometry, giving more confidence that specific dimer interactions are being interrogated in a consistent manner.

Importantly, we have shown that protein L maintains sufficient stability upon insertion of amyloidogenic sequences to fold to a native state. This is significant as the ability of chimeric pL constructs to fold to a native state is integral to the ability to display peptide sequences to reduce non-specific tip-surface interactions.

Whilst the aim of this study was to assess the potential of a scaffold display for SMFS experiments, the study has also yielded intriguing observations on the dimerisation between

αSyn and its less aggregation-prone homologue γSyn, by both SMFS and native ESI-mass spectrometry. Firstly, DFS of the dissociation of pL αSyn_{71-82} dimers revealed a lifetime that is similar to that of full length αSyn (6 and 4 s for pL αSyn_{71-82} and full length αSyn, respectively) measured using the same technique (9). It is important to note, however, that previous SMFS experiments on full length αSyn were conducted at acidic pH where the full length protein is closer to its pI and therefore more prone to aggregation(7; 9; 12; 14; 16; 17). The experiments carried out here were conducted at a more physiological pH (pH 7.5) and are therefore more applicable to the conditions in which the protein self-associates *in vivo*.

To investigate the specificity of the dimer interaction, the dissociation of pL αSyn_{71-82}:pL γSyn_{71-82} heterodimers was also investigated by SMFS. Surprisingly, no reproducible correlation between F_R-L_c values was found for pL γSyn_{71-82} homodimers, suggesting that under the conditions used, dimerisation did not occur or that these dimers dissociated more quickly or at a force that cannot be detected in this experiment. By contrast, dissociation of the αSyn_{71-82}: γSyn_{71-82} heterodimer yielded AFM data that were similar to those obtained for pL αSyn_{71-82} homodimers. Despite this similarity, a population of pL αSyn_{71-82}:pL γSyn_{71-82} dimers inhibits aggregation in the context of both chimeric pL constructs and synthetic peptides equivalent to the central NAC region in isolation. This suggests that the mechanism by which full length γSyn inhibits the aggregation of αSyn(32) may be mediated by the central NAC region of the proteins. As both αSyn and γSyn are highly expressed in many of the same cells of the brain(51), it may be postulated that heterogeneous αSyn and γSyn dimers occur *in vivo* which may chaperone αSyn away from aggregation under normal cellular conditions. The importance of this region to the aggregation of αSyn has been highlighted in a recent

study(52) which shows that αSyn_{71-82} derived peptides bind full length αSyn, and that modified peptides can increase its aggregation.

Together these observations provide further support for the central role of the NAC sequence in the aggregation of full length αSyn. The ability of βSyn to inhibit the aggregation of αSyn, challenges this notion, as this homologue has no NAC region but forms transient interactions with αSyn up- and down-stream from the NAC sequence(32; 53). It is becoming clear that this intrinsically disordered protein displays conformational plasticity and that long range intra- and inter-chain interactions between the termini of this protein, which can be disrupted by changes in pH or mutation, may modulate the interaction potential of NAC(54-56). The development of a facile method that will allow the relative frequency and dissociation rate of these, and other interactions, such as that reported here, may help to understand the early events in the aetiology of αSyn aggregation relevant to Parkinson's disease.

Materials and methods

Expression and purification of pL constructs

pL constructs (Supplementary Figure S1) encoded on pET23a plasmids were expressed in *E. coli* BL21 (DE3) cells. Briefly, overnight starter cultures were used to inoculate 10 x 1L LB medium supplemented with 100 μg/ml ampicillin and grown to an optical density at 600 nm = 0.6. Protein expression was then induced by addition of IPTG to a final concentration of 1 mM. The cultures were allowed to grow for a further 4 h before harvesting. Cell pellets were resuspended in lysis buffer (20 mM Tris.HCl pH 8.0, 300 mM NaCl, 20 mM imidazole, 2 mM DTT, 0.025 % (w/v) sodium azide, 1 mM PMSF, 2 mM benzamidine, 0.15% (v/v) Triton X100, 20 μg/ml DNase and 100 μg/ml lysozyme), homogenised and further lysed by cell disruption at 30K PSI. Cell debris was removed by centrifugation at 18000 x g for 30 min. The proteins

were purified by affinity chromatography using a 5ml His-Trap FF column (GE Healthcare) equilibrated with lysis buffer (without Triton X100, DNase and lysozyme) and eluted by a stepped gradient (25, 50 and 100%) of 20 mM Tris.HCl pH 8.0, 300 mM NaCl, 250 mM imidazole, 2 mM DTT, 0.025 % (w/v) sodium azide, 1 mM PMSF, 2 mM benzamidine. pL complexes were further purified using size exclusion chromatography (HiLoadTM 26/60 Superdex 75 prep grade column, GE Healthcare) equilibrated with 25 mM Tris.HCl, 300 mM NaCl, 2 mM DTT, pH 8. The protein was then dialysed into 20 mM HEPES, pH 7.5 (for pL SMFS experiments) and flash frozen with liquid N_2. The presence, purity and the correct mass of proteins were confirmed by ESI-MS.

Thioflavin T (ThT) aggregation assays

100 µM pL constructs (in 20 mM HEPES, 20 µM ThT, pH 7.5) were incubated at 37 ^{o}C shaking at 600 rpm in a BMG Labtech FLUOstar optima plate reader in Corning 96-well flat bottom assay plates. Plates were sealed with StarSeal advanced polyolefin film (Starlab, Hamburg, Germany). To monitor growth kinetics, samples were excited at 444 nm and the fluorescence emission was monitored at 480 nm with a gain of 1450. Data were accumulated every 6.67 minutes over a period of >100 h.

Synuclein peptides and Thioflavin T (ThT) fluorescence

αSyn_{71-82} and γSyn_{71-82} peptides were purchased from Genscript, NJ, USA at > 99% purity. All peptides were N-terminally acetylated and C-terminally amidated. Peptides were dissolved in 100 % (v/v) HFIP (hexoflouroisopropanol) at 450 µM and dispensed into Corning 96-well flat bottom assay plates. 50 µl was dispensed into wells, and the HFIP was left to evaporate. The

dry peptide in the well was dissolved into 100 µl 20 mM HEPES, 20 µM ThT, pH 7.5 to give a concentration of 225 µM peptide. Incubations were carried out at 37 °C shaking at 600 rpm. Plates were sealed with StarSeal advanced polyolefin film from Starlab, Hamburg, Germany. The fluorescence of the samples were excited at 444 nm and the fluorescence emission was monitored at 480 nm on a BMG Labtech FLUOstar optima plate reader with a gain set at 1450. Where normalised data is presented, it has been processed on the plate reader software and normalised (after buffer subtraction) between 0 and 100. Lag time analysis was carried out by manually fitting a linear regression of the steepest exponential region of the ThT curves on Origin Pro 9.1 software. The fit was extrapolated to calculate the x-intercept (quoted lag times).

^{1}H-^{15}N HSQC NMR spectroscopy

^{1}H-^{15}N HSQC spectra of 400 µM pL αSyn$_{71-82}$ and pL γSyn$_{71-82}$ (20 mM HEPES buffer, 10 % (v/v) D_2O and 0.02% (w/v) sodium azide, pH 7.5) were recorded on an AVANCE III Bruker spectrometer (600 MHz) equipped with a cryogenic probe. Spectra were processed in NMRPipe and analysed in CCPN analysis.

Negative stain transmission electron microscopy (TEM)

Protein samples were pipetted onto the surface of carbon coated copper grids and stained with 1 % (w/v) uranyl acetate. Images were taken on an FEI T12 electron microscope.

AFM surface and cantilever derivatisation

AFM surface and cantilever functionalisation was performed as described previously(43). Prior to an experiment, AFM probes and surfaces were immersed in ~1 ml chloroform containing 20 µl of 250 mM maleimide-PEG-NHS ester (MW 3400 Da, Nanocs NY USA) in DMSO and incubated at room temperature for 1 hour. The PEG linkers used in this study are

polydisperse with masses ± 5% of the stated mass. AFM probes and surfaces were then washed with chloroform and dried with a stream of N_2 gas.

100 µl pL constructs (50 µM in 20 mM HEPES, pH 7.5) containing engineered cysteine residues were deposited over the functionalised surface and AFM probe and left to incubate in a covered container for 30 minutes at room temperature. All proteins analysed by SMFS were immobilised to functionalised probes and surfaces in the presence of 1 mM TCEP (tris(2-carboxyethyl)phosphine) to limit disulphide cross-linkage between proteins. Unreacted protein was then washed from the surface and AFM probe with excess reaction buffer.

Force spectroscopy

All AFM measurements were conducted on an Asylum MFP-3D microscope using Si_3N_4 cantilevers with nominal spring constants of 30 $pNnm^{-1}$ (Bruker MLCT). For each cantilever used, the spring constant was determined using the thermal method(57) using Asylum software. The approach speed was kept constant at 2 μms^{-1}. A retraction speed of 1000 nms^{-1} was used for SMFS experiments that probed the dimerisation of scaffolds. Typically force maps of 500 force-distance curves were taken over a 20 μm^2 area. One dataset typically comprised 4 force maps (2000 force distance curves). All experiments were conducted in 20mM HEPES pH 7.5 at room temperature.

All force spectroscopy data were analysed using IGOR pro 6.32A with an Asylum Research extension (MFP3DXop v30). A force-extension profile was binned for analysis when single characteristic, parabolic WLC events were observed. For each profile, the force (F_R) and contour length (L_C) at rupture was measured. To obtain L_C, each force-extension profile was manually fit to a WLC model(58) (with a fixed persistence length of 0.4 nm, Equation 1).

$$F(x) = \frac{k_B T}{p}\left(0.25\left(1 - \frac{x}{L_C}\right)\right)^2 - 0.25 + \frac{x}{L_C} \quad (1)$$

where F is the entropic restoring force, x is the extension, p is the persistence length, k_B is the Boltzman constant, T is absolute temperature, L_C is the contour length. Hit rates were calculated as the number of hits as a percentage of total approach-retract cycles. The average values over multiple experiments are quoted. The errors on hit rates are the standard deviation between experiments.

Single Gaussian distributions were fit to frequency histograms in order to determine the most probable F_R and L_C for each retraction velocity investigated. For each pulling velocity used, data were collected in triplicate (using a freshly prepared cantilever for each repeat).

To obtain a dynamic force spectrum (DFS), force-extension data were collected using retraction speeds between 200-5000 nms^{-1}. To analyse these data, loading rates were calculated by fitting a WLC model to the rising edge of each unbinding profile when plotted as force versus tip-sample separation. The instantaneous gradient of this fit at rupture (WLC_{slope}) was calculated by inserting the derived contour length and extension at rupture into a differentiated form of the same equation (Equation 2). The loading rate at rupture was then obtained by multiplying this value by the retraction velocity.

$$WLC_{slope} = \frac{k_B T}{p}\left(\frac{1}{2L_c\left(1 - \frac{x}{L_c}\right)^3}\right) + \frac{1}{L_c} \quad (2)$$

where; p is the persistence length, L_C is the contour length, x is the extension, k_B is the Boltzmann constant and T is the temperature.

The natural logarithm of the mean loading rate (Ns^{-1}) at each velocity was plot against the mean rupture force (N) which gives a linear relationship. The Bell-Evans model(44) (Equation 3) was rearranged to use the gradient of the linear fit to calculate the distance from the transition state (x_u) and the y-intercept for the off rate at zero force (k_{off}^{0F})

$$F_R = \left(\frac{k_B T}{x_u}\right) ln \left(\frac{r_f x_u}{k_{off}^{0F} k_B T}\right) \quad (3)$$

where k_B is Bolzmann's constant, T is temperature (in Kelvin), r_f is the rate at which force is loaded onto the complex or loading rate, x_u is the distance from the low energy state to the transition state and k_{off}^{0F} is the spontaneous unfolding or unbinding rate in the absence of force.

Mass spectrometry

A Synapt HDMS quadrupole-time-of-flight mass spectrometer (Waters Corpn., Manchester, UK), equipped with a Triversa NanoMate (Advion Biosciences, Ithaca, NY, USA) automated nano-ESI interface, was used for these analyses. The instrument has a travelling-wave IMS device situated between the quadrupole and the time-of-flight analysers.

αSyn and γSyn peptide samples an pL chimeric constructs (100 µM final concentration in 100 mM ammonium acetate buffer, pH 6.8) were analysed using positive mode nanoESI with a capillary voltage of 1.7 kV and a nitrogen nebulising gas pressure of 0.8 psi. The following instrumental parameters were used: cone voltage 30 V; source temperature 60 °C; backing

pressure 3.2 mBar; ramped travelling wave height 7–20 V; travelling wave speed 300 ms^{-1}; IMS cell pressure 0.55 mBar. Data were acquired over the range m/z 500–6,000. Data were processed by use of MassLynx v4.1 and Driftscope v2.4 software supplied with the mass spectrometer. Mass calibration was achieved using caesium iodide solution, prepared by dissolving the compound in 50 % (*v/v*) water/ isopropanol to a concentration of 2 mg/ml.

Circular dichroism (CD)

Far UV (190-260 nm) CD spectroscopy was performed on 50 µM pL constructs (25 mM sodium phosphate buffer, 2 mM DTT, pH 8.0) in a 1 mm path length curvette (Hellma) using a ChirascanTM plus CD Spectrometer (Applied Photophysics, U.K.). CD spectra were acquired using a 1 nm bandwidth at room temperature, 1 s time step. Three scans were taken per sample.

For thermal denaturation experiments, a temperature gradient from 20 to 90 ^{o}C in 1 ^{o}C steps was performed. Protein samples were incubated for 180 s at each temperature before CD spectra were taken as above. The thermal melt data were analysed on Photophysics Global3 software.

Fluorescence spectroscopy

Intrinsic tryptophan emission spectra of 50 µM pL constructs (25 mM sodium phosphate buffer, 2mM DTT, pH 8.0) were measured on a Photon Technology International fluorometer (Ford, West Sussex, UK). Excitation and emission slit widths were set to 1 and 2 nm, respectively. Proteins were excited at 280 nm and emission spectra were recorded at 290-400 nm. Spectra were recorded of three replicates. All data were normalised to the unfolded

state. The unfolded state was recorded in the same conditions as above in the presence of 8M urea.

Supplementary material

Supplementary figures and tables are included in the file Supplementary_Material.docx

Acknowledgments

The authors acknowledge funding of BBSRC BRIC case studentship to CPAD (BB/K02101X/1), and the support of the European Research Council under the European Union's Seventh Framework Programme FP7.2007-2013/Grant agreement number 322408. We thank the Wellcome Trust (grant code 094232) for the purchase of a Chiroscan CD spectrometer and the Wellcome Trust (grant code 094232) and the University of Leeds for funding the NMR instrumentation. The Synapt HDMS mass spectrometer was purchased with funds from the BBSRC (BB/E012558/1).

Figure Legends

Figure 1. Using pL as a peptide-presenting scaffold. (A) Structural model of the pL scaffold. The β3-β4 loop, peptide insert and Cys residue for immobilisation are shown in grey, blue and red, respectively. The β3-β4 loop was extended using SWISS-MODEL and the PDB file 1HZ6(59)). (B) Measuring chimeric pL dimer dissociation using the AFM. The derivitised AFM tip is brought into contact with a similarly derivitised surface (1) allowing dimerisation via the guest peptide. The complex is then extended by retracting the cantilever, the force generated bends the cantilever and reaches a maximum (2) at complex dissociation (rupture force (F_R)) prior to relaxation (3). (C) Typical force-extension profile of the force induced dissociation of a mechanically resistant dimer. The positions of dimerisaton (1), dissociation (2) and relaxation (3) are shown. The contour length (L_C) and F_R are measured for each dissociation event, the latter parameter obtained by fitting the Worm Like Chain (WLC) model (black curve) to the profile (Materials and Methods).

Figure 2. pL αSyn$_{71-82}$ and pL GS have similar structures as revealed by HSQC NMR. The data presented shows 600 MHz ^{1}H-^{15}N HSQC-NMR spectra of ^{15}N labelled pL αSyn$_{71-82}$ and pL GS. (A) Overlaid spectra of pL GS (red peaks) and pL αSyn$_{71-82}$ (blue peaks). Both spectra have dispersed and well defined peaks characteristic of folded proteins. Additional peaks observed for pL αSyn$_{71-82}$ at ~8 ppm in the ^{1}H dimension most likely arise from residues in the inserted peptide in an unfolded conformation. (B) Expanded region highlighting additional peaks that are observed for pL αSyn$_{71-82}$ in the region of the spectrum consistent with inserted peptide having an unfolded dynamic conformation. A small number of residues showing chemical shift perturbations are also highlighted (blue dashed boxes). Shifts arise because residues form part of, or are close to, the β3-β4 loop.

Figure 3. SMFS can detect dissociation events for pL αSyn$_{71-82}$ but not pL GS. Schematic (left), sample force extension profiles (middle) and a F_R versus L_c scattergram (right, rendered as a contour plot and showing the associated L_c and F_R frequency-histograms above and to the side, respectively for (A) pL αSyn$_{71-82}$ and (B) pL GS dissociation events. WLC fits (black line) are fit to the force-extension profiles. The contour plot for pL αSyn$_{71-82}$ shows a "hotspot" of reproducible and correlated L_C and F_R values. No "hotspot" is visible for pL GS dissociation events. The total number of force-retract cycles (total triplicate) are 8000 and 2500 for pL αSyn$_{71-82}$ and pL GS dimerisation interactions, respectively.

Figure 4. Using dynamic force spectroscopy to investigate αSyn$_{71-82}$ dissociation. (A) Schematic representation of an unbinding energy landscape. The dotted line depicts the tilted energy landscape under force. x_U is depicted as the distance from the bound energy well to the transition state. k_{off}^{0F} is shown as the stochastic process of crossing the transition energy

barrier. (B) Dynamic force spectrum of αSyn$_{71-82}$ dissociation. Data (mean of the triplicate datasets, error bars are the standard deviation) are fitted to the Bell-Evans model(44; 45) to obtain values k_{off}^{0F} and x_U (shown inset). The errors of the k_{off}^{0F} and x_U were calculated by manual bootstrapping. The total number of approach retract cycles (total triplicate) for pL αSyn$_{71-82}$ dimer dissociation events are 5200, 5500, 6500, 6000 and 5500 for pulling speeds 200, 500, 1000, 3000 and 5000 nms^{-1}, respectively.

Figure 5. SMFS can detect dissociation events for pL αSyn$_{71-82}$: pL γSyn$_{71-82}$ heterodimers but not pL γSyn$_{71-82}$ homodimers. Schematic (left), sample force extension profiles (middle) and a F_R versus L_c contour plot (right), showing the associated L_c and F_R frequency-histograms above and to the side, respectively for (A) pL γSyn$_{71-82}$ homodimer dissociation events and (B) pL αSyn$_{71-82}$:pL γSyn$_{71-82}$ heterodimer dissociation events. WLC fits (black line) are fit to force extension profiles. While no "hotspot" is visible for the dissociation of pL γSyn$_{71-82}$ homodimers, the contour plot for dissociation of the heterodimer shows a "hotspot" of reproducible and correlated L_C and F_R values. The modal L_C and F_R were calculated to be 19 ± 1 nm and 53 ± 1 pN, respectively. The total number of approach retract cycles (total triplicate) for pL γSyn$_{71-82}$ homodimerisation and αSyn$_{71-82}$/ γSyn$_{71-82}$ heterodimerisation interactions are both 2500.

Figure 6. Dimeric species of chimeric pL constructs analysed by ESI-MS. ESI-mass spectra showing two different charge states (7+ and 9+) of the dimeric species formed after 4h incubation of pL GS (pink), pL αSyn$_{71-82}$ (blue), pL γSyn$_{71-82}$ (orange) and 1:1 pL αSyn$_{71-82}$ and pL γSyn$_{71-82}$ (heterodimer coloured green). The numbers denote the oligomer order, with the positive-charge state of ions in superscript. The spectra of pL GS shows the absence of dimer

after 4h. The difference in mass between pL αSyn_{71-82} and pL γSyn_{71-82} allows pL αSyn_{71-82} and pL γSyn_{71-82} homodimers and heterodimeric species to be readily discerned from one another.

Figure 7. ThT fibril formation assays show that pL αSyn_{71-82} inhibits the aggregation of pL γSyn_{71-82}. ThT fluorescence assay showing the normalised fluorescence over time of pL αSyn_{71-82} (blue), pL γSyn_{71-82} (orange), pL GS (pink) and the 1:1 mix of pL αSyn_{71-82} and pL γSyn_{71-82} (green). Proteins were incubated at 37 °C, 600 rpm at a final concentration of 100 µM (α/γ mix at 50µM of each protein).

Conflict of Interest Statement

The authors declare no conflicts of interest.

References

1. Dobson CM (2003) Protein folding and misfolding. Nature 426:884-890.
2. Dobson CM (2004) Principles of protein folding, misfolding and aggregation. Semin Cell Dev Biol 15:3-16.
3. Knowles TPJ, Vendruscolo M, Dobson CM (2014) The amyloid state and its association with protein misfolding diseases. Nat Rev Mol Cell Biol 15:384-396.
4. Verma M, Vats A, Taneja V (2015) Toxic species in amyloid disorders: oligomers or mature fibrils. Ann Indian Acad Neurol 18:138-145.
5. Cremades N, Cohen SIA, Deas E, Abramov AY, Chen AY, Orte A, Sandal M, Clarke RW, Dunne P, Aprile FA, Bertoncini CW, Wood NW, Knowles TPJ, Dobson CM, Klenerman D (2012) Direct observation of the interconversion of normal and toxic forms of alpha-synuclein. Cell 149:1048-1059.
6. Lv ZJ, Krasnoslobodtsev AV, Zhang YL, Ysselstein D, Rochet JC, Blanchard SC, Lyubchenko YL (2015) Direct detection of alpha-synuclein dimerization dynamics: single-molecule fluorescence analysis. Biophys J 108:2038-2047.
7. McAllister C, Karymov MA, Kawano Y, Lushnikov AY, Mikheikin A, Uversky VN, Lyubchenko YL (2005) Protein interactions and misfolding analyzed by AFM force spectroscopy. J Mol Biol 354:1028-1042.
8. Sandal M, Valle F, Tessari I, Mammi S, Bergantino E, Musiani F, Brucale M, Bubacco L, Samori B (2008) Conformational equilibria in monomeric alpha-synuclein at the single-molecule level. PLoS Biol 6:99-108.
9. Yu JP, Malkova S, Lyubchenko YL (2008) Alpha-synuclein misfolding: single molecule AFM force spectroscopy study. J Mol Biol 384:992-1001.
10. Brucale M, Sandal M, Di Maio S, Rampioni A, Tessari I, Tosatto L, Bisaglia M, Bubacco L, Samori B (2009) Pathogenic mutations shift the equilibria of alpha-synuclein single molecules towards structured conformers. ChemBioChem 10:176-183.
11. Dougan L, Li J, Badilla CL, Berne BJ, Fernandez JM (2009) Single homopolypeptide chains collapse into mechanically rigid conformations. Proc Nat Acad Sci 106:12605-12610.
12. Yu JP, Lyubchenko YL (2009) Early stages for parkinson's development: alpha-synuclein misfolding and aggregation. J Neuroimmune Pharm 4:10-16.
13. Kim BH, Palermo NY, Lovas S, Zaikova T, Keana JFW, Lyubchenko YL (2011) Single-molecule atomic force microscopy force spectroscopy study of amyloid beta-40 interactions. Biochem 50:5154-5162.
14. Yu JP, Warnke J, Lyubchenko YL (2011) Nanoprobing of alpha-synuclein misfolding and aggregation with atomic force microscopy. Nanomed Nanotech Biol Med 7:146-152.
15. Hervas R, Oroz J, Galera-Prat A, Goni O, Valbuena A, Vera AM, Gomez-Sicilia A, Losada-Urzaiz F, Uversky VN, Menendez M, Laurents DV, Bruix M, Carrion-Vazquez M (2012) Common features at the start of the neurodegeneration cascade. PLoS Biol 10.
16. Krasnoslobodtsev AV, Peng J, Asiago JM, Hindupur J, Rochet JC, Lyubchenko YL (2012) Effect of spermidine on misfolding and interactions of alpha-synuclein. Plos One 7.
17. Krasnoslobodtsev AV, Volkov IL, Asiago JM, Hindupur J, Rochet JC, Lyubchenko YL (2013) Alpha-synuclein misfolding assessed with single molecule AFM force spectroscopy: effect of pathogenic mutations. Biochem 52:7377-7386.
18. Yu H, Liu X, Neupane K, Gupta AN, Brigley AM, Solanki A, Sosova I, Woodside MT (2012) Direct observation of multiple misfolding pathways in a single prion protein molecule. Proc Nat Acad Sci 109:5283-5288.

19. Lee CK, Wang YM, Huang LS, Lin SM (2007) Atomic force microscopy: determination of unbinding force, off rate and energy barrier for protein-ligand interaction. Micron 38:446-461.
20. Farrance OE, Paci E, Radford SE, Brockwell DJ (2015) Extraction of accurate biomolecular parameters from single-molecule force spectroscopy experiments. ACS Nano 9:1315-1324.
21. Tong ZH, Mikheikin A, Krasnoslobodtsev A, Lv ZJ, Lyubchenko YL (2013) Novel polymer linkers for single molecule AFM force spectroscopy. Methods 60:161-168.
22. Lv ZJ, Roychaudhuri R, Condron MM, Teplow DB, Lyubchenko YL (2013) Mechanism of amyloid beta-protein dimerization determined using single-molecule AFM force spectroscopy. Sci Rep 3.
23. Ueda K, Fukushima H, Masliah E, Xia Y, Iwai A, Yoshimoto M, Otero DAC, Kondo J, Ihara Y, Saitoh T (1993) Molecular-cloning of cDNA-encoding an unrecognized component of amyloid in Alzheimer Disease. Proc Natl Acad Sci USA 90:11282-11286.
24. Giasson BI, Murray IVJ, Trojanowski JQ, Lee VMY (2001) A hydrophobic stretch of 12 amino acid residues in the middle of alpha-synuclein is essential for filament assembly. J Biol Chem 276:2380-2386.
25. Walder R, LeBlanc M-A, Van Patten WJ, Edwards DT, Greenberg JA, Adhikari A, Okoniewski SR, Sullan RMA, Rabuka D, Sousa MC, Perkins TT (2017) Rapid characterization of a mechanically labile α-helical protein enabled by efficient site-specific bioconjugation. J Am Chem Soc 139:9867-9875.
26. Oroz J, Hervas R, Carrion-Vazquez M (2012) Unequivocal single-molecule force spectroscopy of proteins by AFM using pFS vectors. Biophys J 102:682-690.
27. Krasnoslobodtsev AV, Zhang YL, Viazovkina E, Gall A, Bertagni C, Lyubchenko YL (2015) A flexible nanoarray approach for the assembly and probing of molecular complexes. Biophys J 108:2333-2339.
28. Maity S, Viazovkina E, Gall A, Lyubchenko YL (2017) Single-molecule probing of amyloid nano-ensembles using the polymer nanoarray approach. Phys Chem Chem Phys 19:16387-16394.
29. Vera AM, Carrion-Vazquez M (2016) Direct identification of protein-protein interactions by single-molecule force spectroscopy. Angewandte Chemie (International ed in English) 55:13970-13973.
30. Tuttle MD, Comellas G, Nieuwkoop AJ, Covell DJ, Berthold DA, Kloepper KD, Courtney JM, Kim JK, Barclay AM, Kendall A, Wan W, Stubbs G, Schwieters CD, Lee VMY, George JM, Rienstra CM (2016) Solid-state NMR structure of a pathogenic fibril of full-length human alpha-synuclein. Nat Struct Mol Biol 23:409-415.
31. Biere AL, Wood SJ, Wypych J, Steavenson S, Jiang YJ, Anafi D, Jacobsen FW, Jarosinski MA, Wu GM, Louis JC, Martin F, Narhi LO, Citron M (2000) Parkinson's disease-associated alpha-sylnuclein is more fibrillogenic than beta- and gamma-synuclein and cannot cross-seed its homologs. J Biol Chem 275:34574-34579.
32. Uversky VN, Li J, Souillac P, Millett IS, Doniach S, Jakes R, Goedert M, Fink AL (2002) Biophysical properties of the synucleins and their propensities to fibrillate - inhibition of alpha-synuclein assembly by beta- and gamma-synucleins. J Biol Chem 277:11970-11978.
33. Smith DP, Giles K, Bateman RH, Radford SE, Ashcroft AE (2007) Monitoring copopulated conformational states during protein folding events using Electrospray ionization-ion mobility spectrometry-mass spectrometry. J Am Soc Mass Spectrom 18:2180-2190.

34. Woods LA, Platt GW, Hellewell AL, Hewitt EW, Homans SW, Ashcroft AE, Radford SE (2011) Ligand binding to distinct states diverts aggregation of an amyloid-forming protein. Nat Chem Biol 7:730-739.
35. Young LM, Cao P, Raleigh DP, Ashcroft AE, Radford SE (2014) Ion mobility spectrometry-mass spectrometry defines the oligomeric intermediates in amylin amyloid formation and the mode of action of inhibitors. J Am Chem Soc 136:660-670.
36. Young LM, Mahood RA, Saunders JC, Tu LH, Raleigh DP, Radford SE, Ashcroft AE (2015) Insights into the consequences of co-polymerisation in the early stages of IAPP and amyloid beta peptide assembly from mass spectrometry. Analyst 14:6990-6999.
37. Young LM, Saunders JC, Mahood RA, Revill CH, Foster RJ, Ashcroft AE, Radford SE (2016) ESI-IMS-MS: A method for rapid analysis of protein aggregation and its inhibition by small molecules. Methods 95:62-69.
38. Minard P, Scalley-Kim M, Watters A, Baker D (2001) A "loop entropy reduction" phage-display selection for folded amino acid sequences. Protein Sci 10:129-134.
39. Brockwell DJ, Beddard GS, Paci E, West DK, Olmsted PD, Smith DA, Radford SE (2005) Mechanically unfolding the small, topologically simple protein L. Biophys J 89:506-519.
40. Sadler DP, Petrik E, Taniguchi Y, Pullen JR, Kawakami M, Radford SE, Brockwell DJ (2009) Identification of a mechanical rheostat in the hydrophobic core of protein L. J Mol Biol 393:237-248.
41. Aden J, Wittung-Stafshede P (2014) Folding of an unfolded protein by macromolecular crowding in vitro. Biochem 53:2271-2277.
42. Marko JF, Siggia ED (1995) Stretching DNA. Macromolecules 28:8759-8770.
43. Hickman SJ, Cooper REM, Bellucci L, Paci E, Brockwell DJ (2017) Gating of TonB-dependent transporters by substrate-specific forced remodelling. Nat Commun 8.
44. Evans E, Ritchie K (1997) Dynamic strength of molecular adhesion bonds. Biophys J 72:1541-1555.
45. Evans E (2001) Probing the relation between force - lifetime - and chemistry in single molecular bonds. Annu Rev Biophys Biomol Struct 30:105-128.
46. Erba EB, Petosa C (2015) The emerging role of native mass spectrometry in characterizing the structure and dynamics of macromolecular complexes. Protein Sci 24:1176-1192.
47. Morel B, Varela L, Azuaga AI, Conejero-Lara F (2010) Environmental conditions affect the kinetics of nucleation of amyloid fibrils and determine their morphology. Biophys J 99:3801-3810.
48. Buell AK, Galvagnion C, Gaspar R, Sparr E, Vendruscolo M, Knowles TP, Linse S, Dobson CM (2014) Solution conditions determine the relative importance of nucleation and growth processes in alpha-synuclein aggregation. Proc Natl Acad Sci U S A 111:7671-7676.
49. Tipping KW, Karamanos TK, Jakhria T, Iadanza MG, Goodchild SC, Tuma R, Ranson NA, Hewitt EW, Radford SE (2015) pH-induced molecular shedding drives the formation of amyloid fibril-derived oligomers. Proc Nat Acad Sci 112:5691.
50. Celik E, Moy VT (2012) Nonspecific interactions in AFM force spectroscopy measurements. Journal of molecular recognition : JMR 25:53-56.
51. George JM (2002) The synucleins. Genome Biol 3.

52. Jha NN, Ranganathan S, Kumar R, Mehra S, Panigrahi R, Navalkar A, Ghosh D, Kumar A, Padinhateeri R, Maji SK (2017) Complexation of NAC-derived peptide ligands with the C-Terminus of alpha-Synuclein accelerates its aggregation. Biochem.
53. Janowska MK, Wu KP, Baum J (2015) Unveiling transient protein-protein interactions that modulate inhibition of alpha-synuclein aggregation by beta-synuclein, a pre-synaptic protein that co-localizes with alpha-synuclein. Sci Rep 5.
54. Bertoncini CW, Fernandez CO, Griesinger C, Jovin TM, Zweckstetter M (2005) Familial mutants of alpha-synuclein with increased neurotoxicity have a destabilized conformation. J Biol Chem 280:30649-30652.
55. Bertoncini CW, Jung YS, Fernandez CO, Hoyer W, Griesinger C, Jovin TM, Zweckstetter M (2005) Release of long-range tertiary interactions potentiates aggregation of natively unstructured alpha-synuclein. Proc Natl Acad Sci USA 102:1430-1435.
56. Cho MK, Nodet G, Kim HY, Jensen MR, Bernado P, Fernandez CO, Becker S, Blackledge M, Zweckstetter M (2009) Structural characterization of alpha-synuclein in an aggregation prone state. Protein Sci 18:1840-1846.
57. Hutter JL, Bechhoefer J (1993) Calibration of atomic-force microscope tips. Rev Sci Instrum 64:1868-1873.
58. Bustamante C, Marko JF, Siggia ED, Smith S (1994) Entropic elasticity of lambda-phage DNA. Science 265:1599-1600.
59. O'Neill JW, Kim DE, Baker D, Zhang KYJ (2001) Structures of the B1 domain of protein L from Peptostreptococcus magnus with a tyrosine to tryptophan substitution. Acta Cryst D 57:480-487.

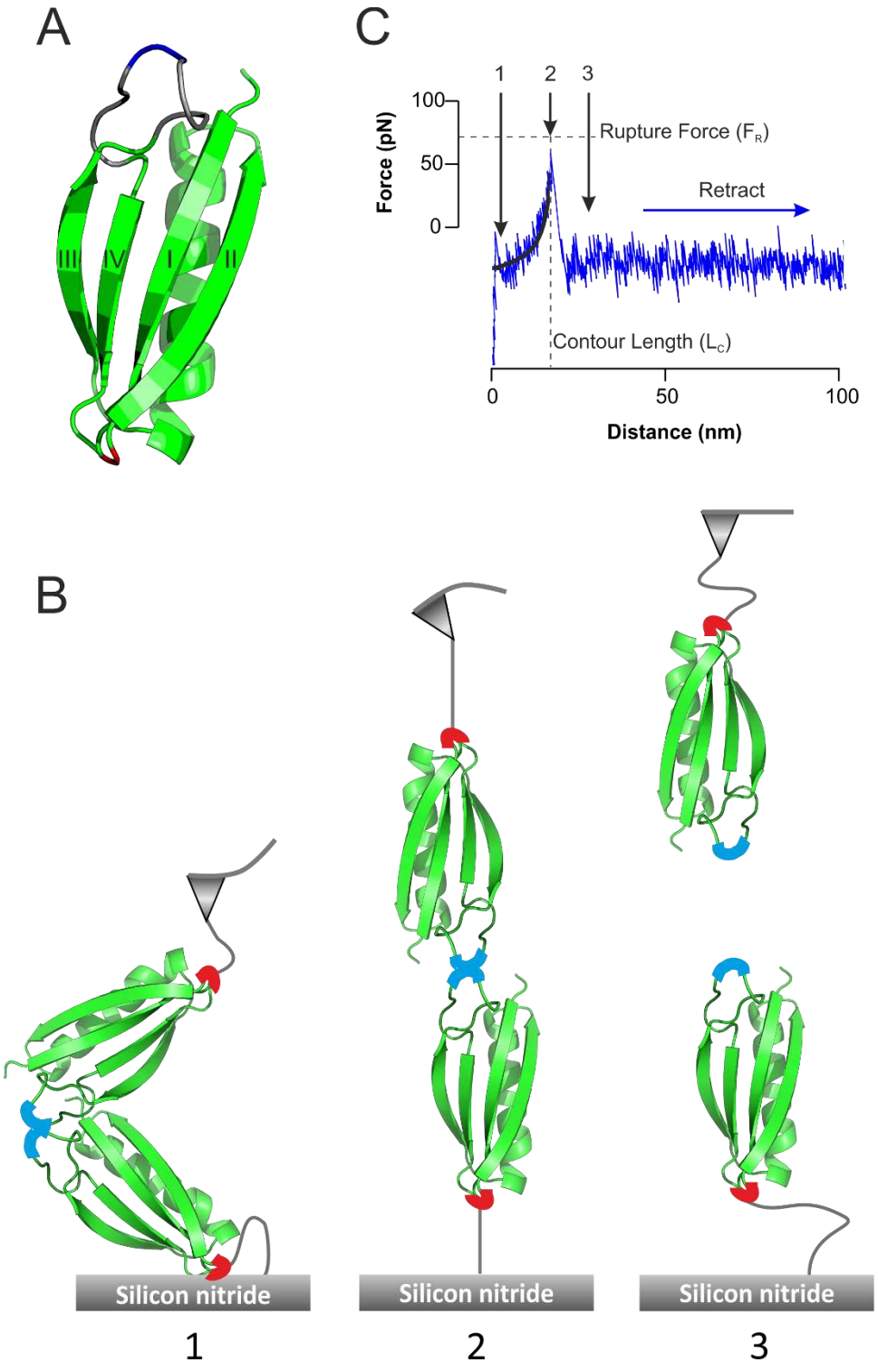
A
III
IV
I
II
C
1
2
3
100
50
0
Force (pN)
Rupture Force (F_R)
Retract
Contour Length (L_c)
0
50
100
Distance (nm)
B
Silicon nitride
Silicon nitride
Silicon nitride
1
2
3

Figure 1

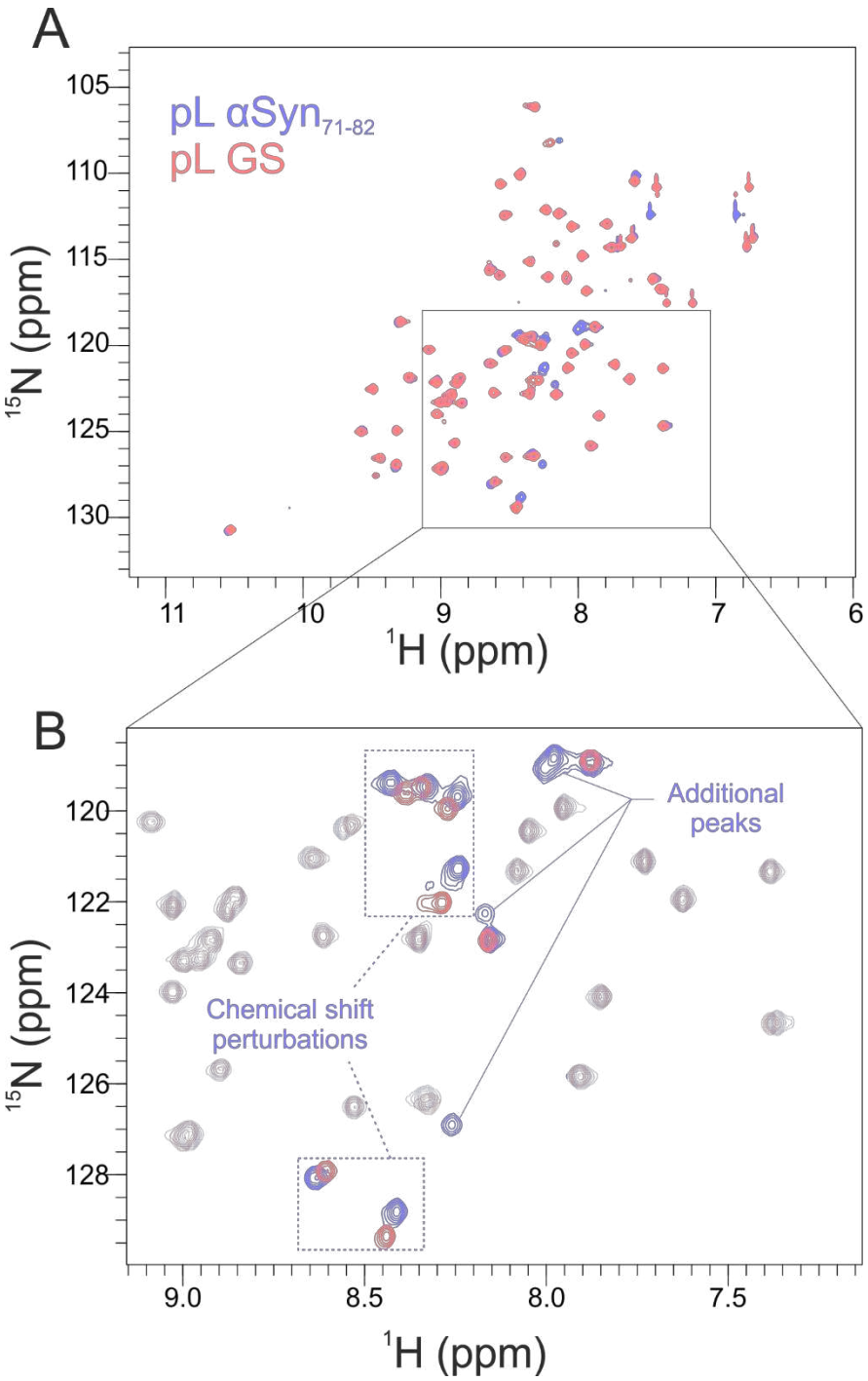
A
pL αSyn71-82
pL GS
105
110
115
120
125
130
15N (ppm)
11
10
9
8
7
6
1H (ppm)
B
120
122
124
126
128
15N (ppm)
Additional peaks
Chemical shift perturbations
9.0
8.5
8.0
7.5
1H (ppm)

Figure 2

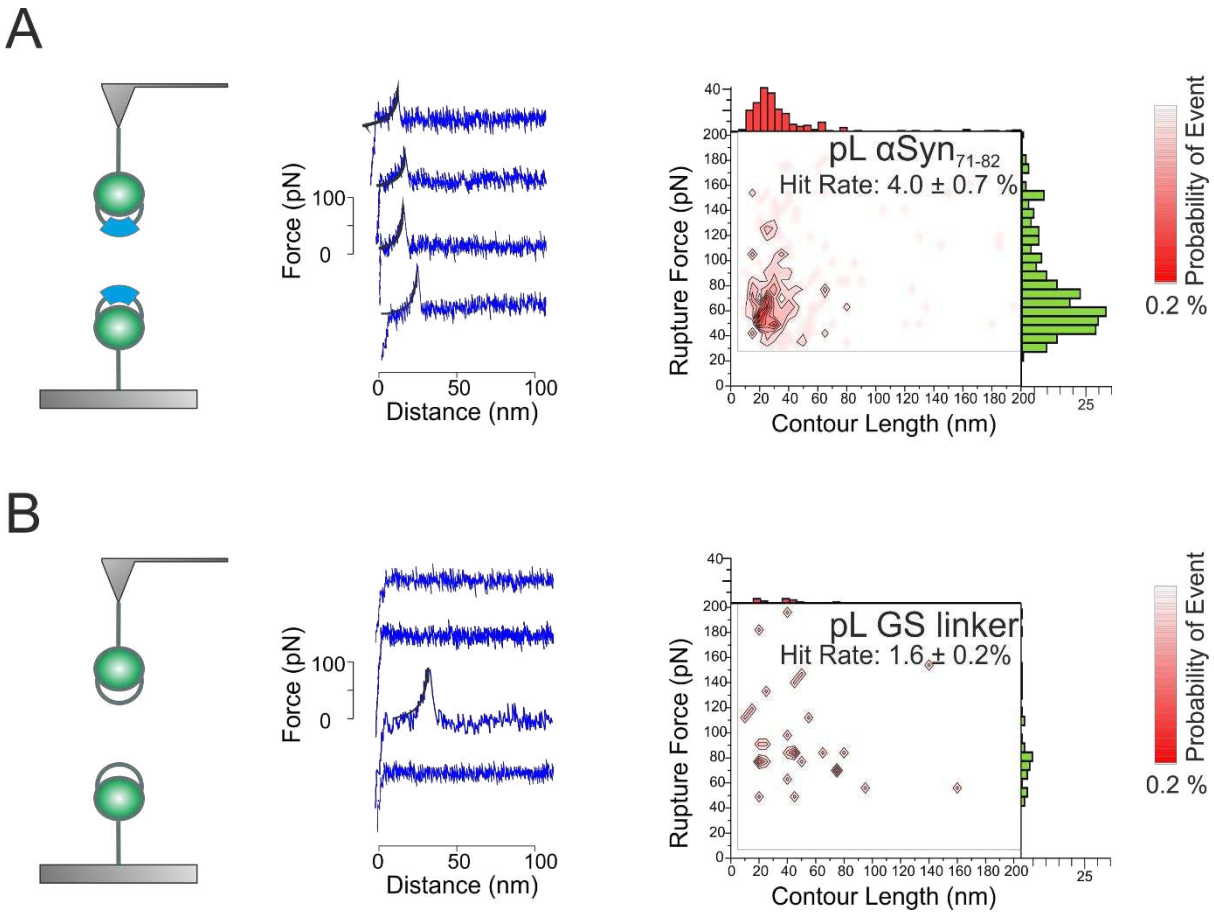
A
Force (pN)
100
0
0
50
100
Distance (nm)
pL αSyn71-82
Hit Rate: 4.0 ± 0.7 %
Rupture Force (pN)
Contour Length (nm)
Probability of Event
0.2 %
B
Force (pN)
100
0
0
50
100
Distance (nm)
pL GS linker
Hit Rate: 1.6 ± 0.2%
Rupture Force (pN)
Contour Length (nm)
Probability of Event
0.2 %

Figure 3

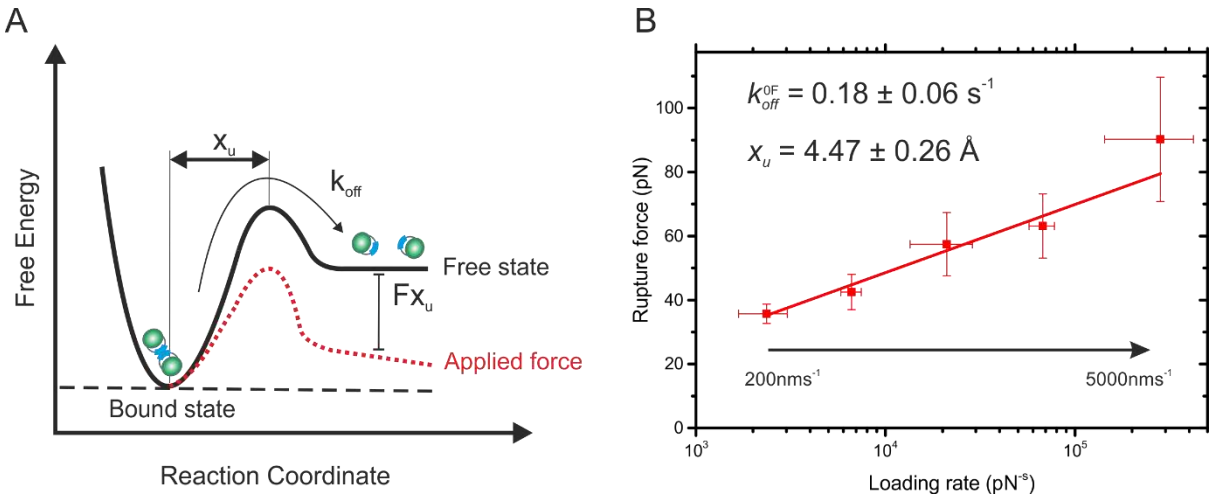
A
Free Energy
x_u
k_{off}
Free state
Fx_u
Applied force
Bound state
Reaction Coordinate
B
k_{off}^{0F} = 0.18 ± 0.06 s^{-1}
x_u = 4.47 ± 0.26 Å
Rupture force (pN)
100
80
60
40
20
0
200nms^{-1}
5000nms^{-1}
10^3
10^4
10^5
Loading rate (pN^{-s})

Figure 4

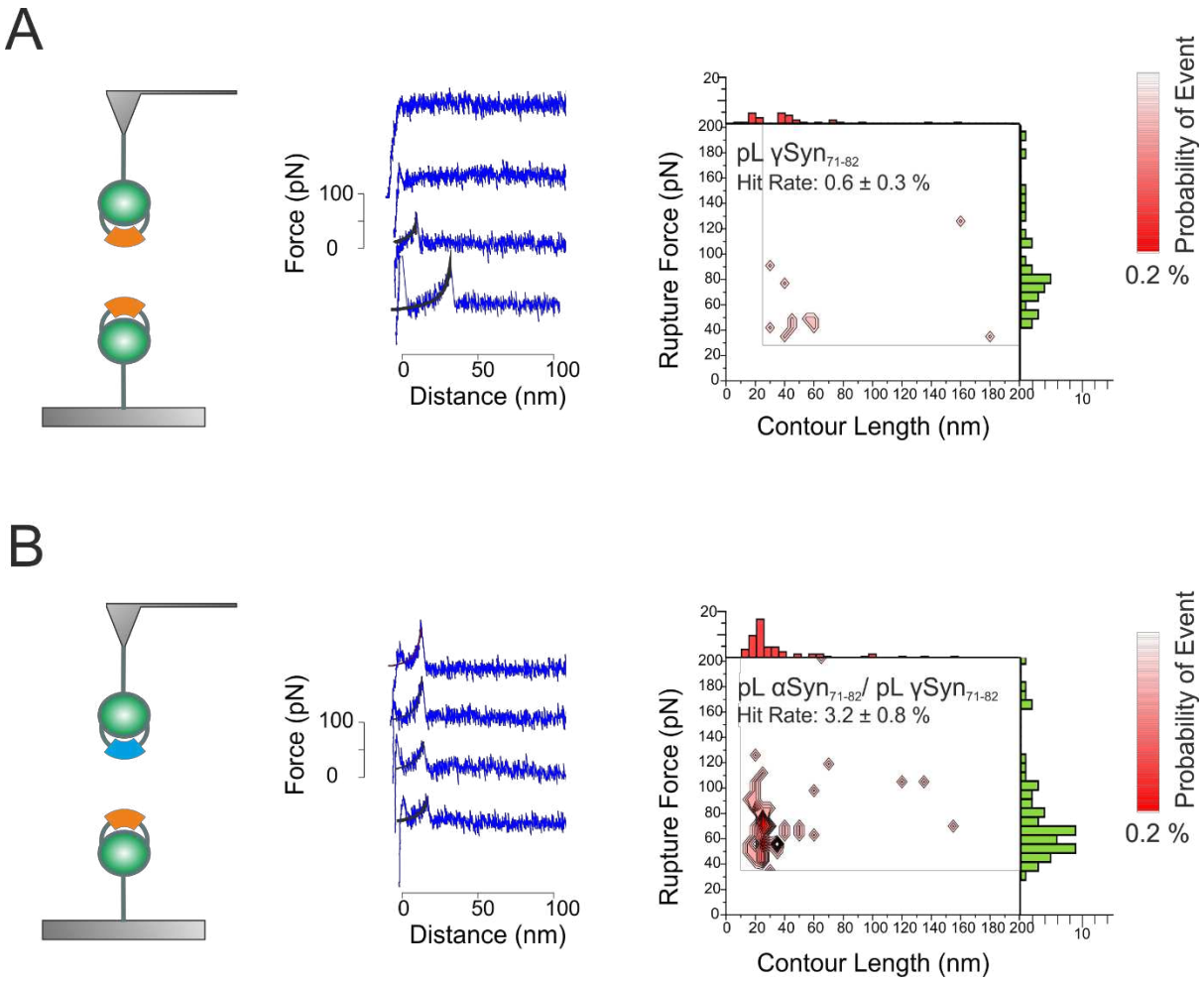
A
Force (pN)
100
0
0
50
100
Distance (nm)
Rupture Force (pN)
pL γSyn71-82
Hit Rate: 0.6 ± 0.3 %
Contour Length (nm)
Probability of Event
0.2 %
B
Force (pN)
100
0
0
50
100
Distance (nm)
Rupture Force (pN)
pL αSyn71-82/ pL γSyn71-82
Hit Rate: 3.2 ± 0.8 %
Contour Length (nm)
Probability of Event
0.2 %

Figure 5

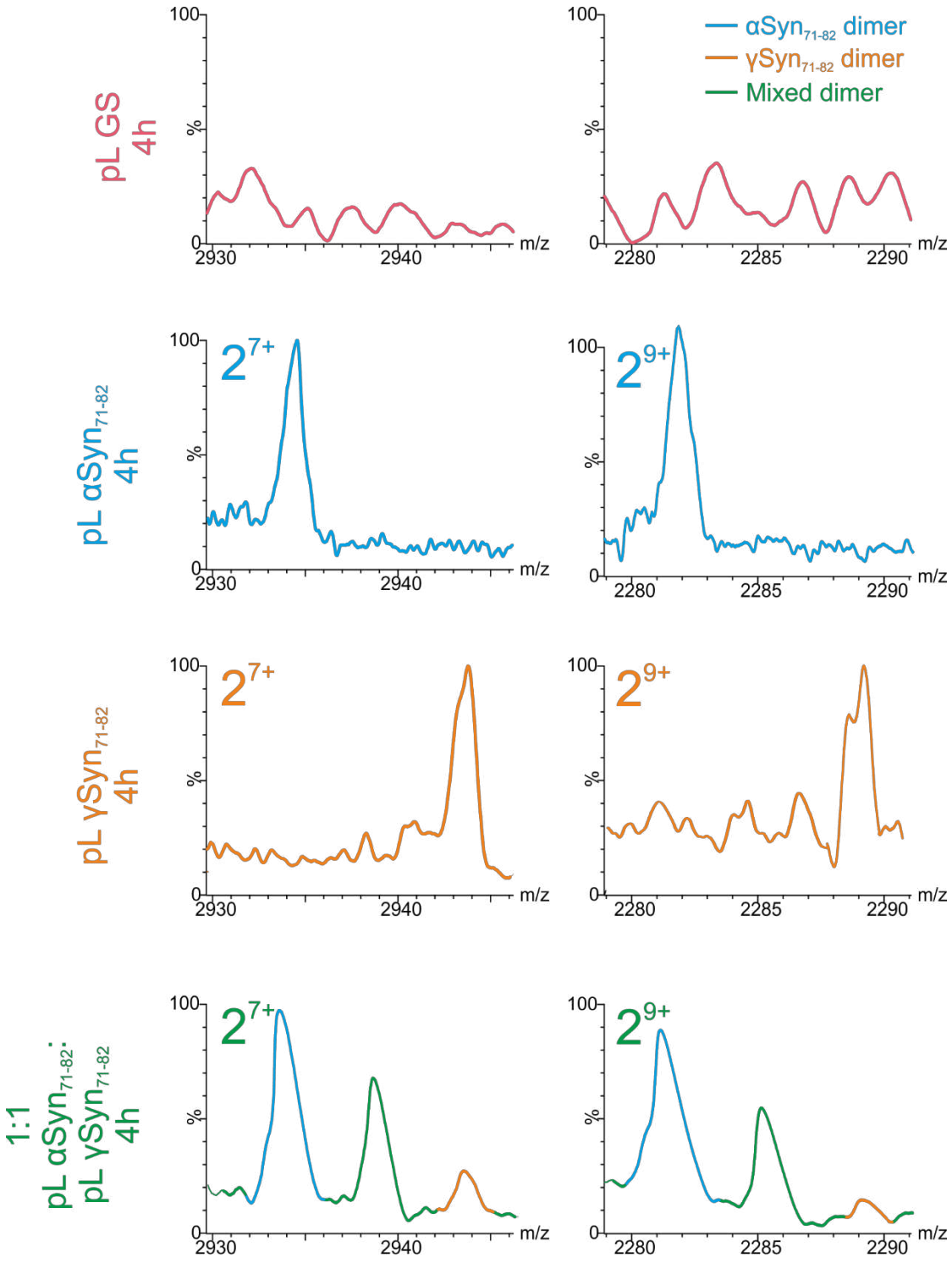
pL GS 4h
pL αSyn71-82 4h
pL γSyn71-82 4h
1:1 pL αSyn71-82 : pL γSyn71-82 4h
αSyn71-82 dimer
γSyn71-82 dimer
Mixed dimer
100
%
0
m/z
2930
2940
2280
2285
2290
2 7+
2 9+

Figure 6

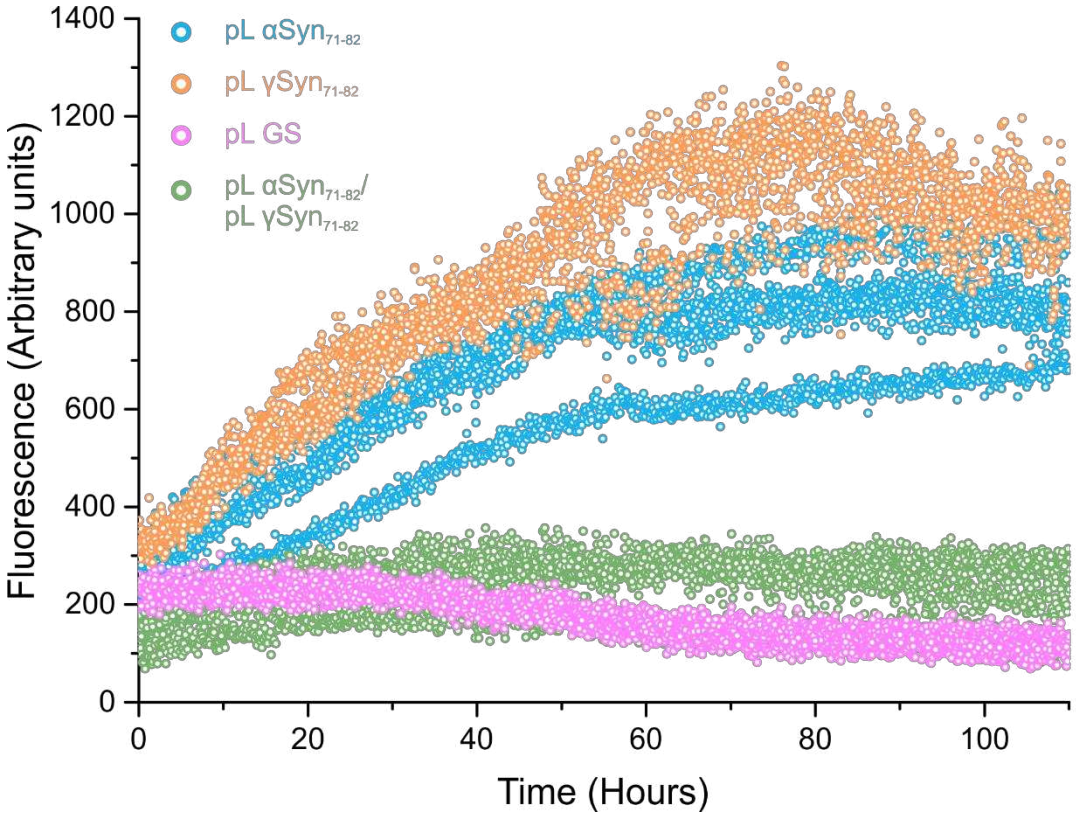
pL αSyn71-82
pL γSyn71-82
pL GS
pL αSyn71-82/
pL γSyn71-82
Fluorescence (Arbitrary units)
Time (Hours)
0
200
400
600
800
1000
1200
1400
0
20
40
60
80
100

Figure 7

Supplementary Material

Supplementary figures

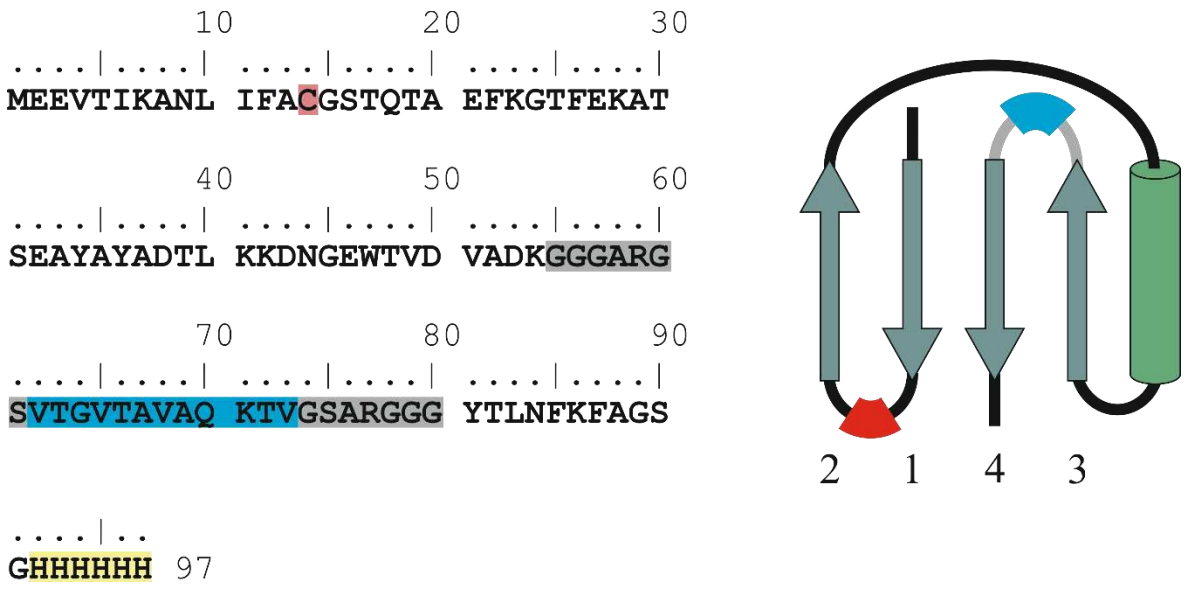

Figure S1. Sequence and topology of pL αSyn$_{71-82}$.

Left: primary sequence of pL αSyn$_{71-82}$. The sequences and position of the β3-β4 loop extension and the inserted αSyn$_{71-82}$ peptide are highlighted in grey and blue, respectively. Peptide sequences for γSyn$_{71-82}$ and the non-aggregation control (GS)$_6$ were inserted at the same position as αSyn$_{71-82}$. The engineered cysteine residue used for immobilisation is highlighted in red. Yellow highlighted text indicates the presence of a (His)$_6$ tag to enable Ni^{2+}-affinity purification. Right: structural schematic showing the position of the engineered cysteine residue used for immobilisation (red) relative to the position of the guest peptide (blue) with the extended β3-β4 loop (pale grey). Extension by the blue and red regions would shear the mechanically strong interface (β-strands 1 and 4).

Figure S2. Sequence alignment of the central NAC regions of α- and γ-synuclein.

Residue properties are colour coded: red (hydrophobic), blue (polar) and yellow (charged). The sequences are highly homologous, 7/12 residues are identical and 3 of the 5 substitutions are conservative.

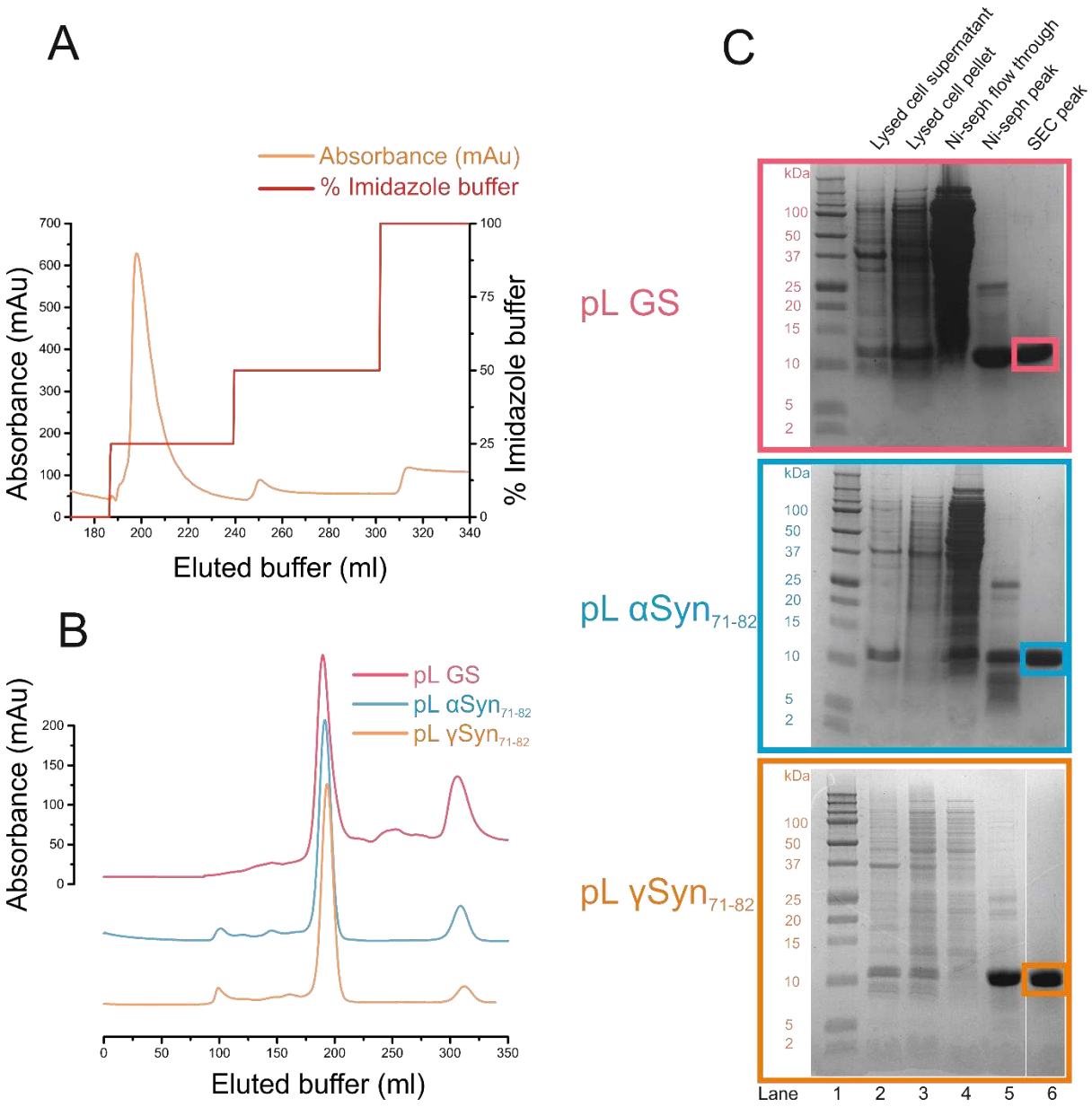

Figure S3. Two-step purification of pL variants.

(A) Typical elution profile for the Ni^{2+}-Sepharose affinity chromatography step (pL γSyn$_{71-82}$). The protein eluted in 25 % imidazole is visualised in the fifth lane in each gel in (C). (B) Elution profiles of the size exclusion chromatography step (SEC). The final purified protein after SEC is shown in lane 6 of the gels shown in (C), highlighted with a coloured box. (C) SDS-polyacylamide gels following the purification of pL GS (pink), pL αSyn$_{71-82}$ (blue) and pL γSyn$_{71-82}$ (orange).

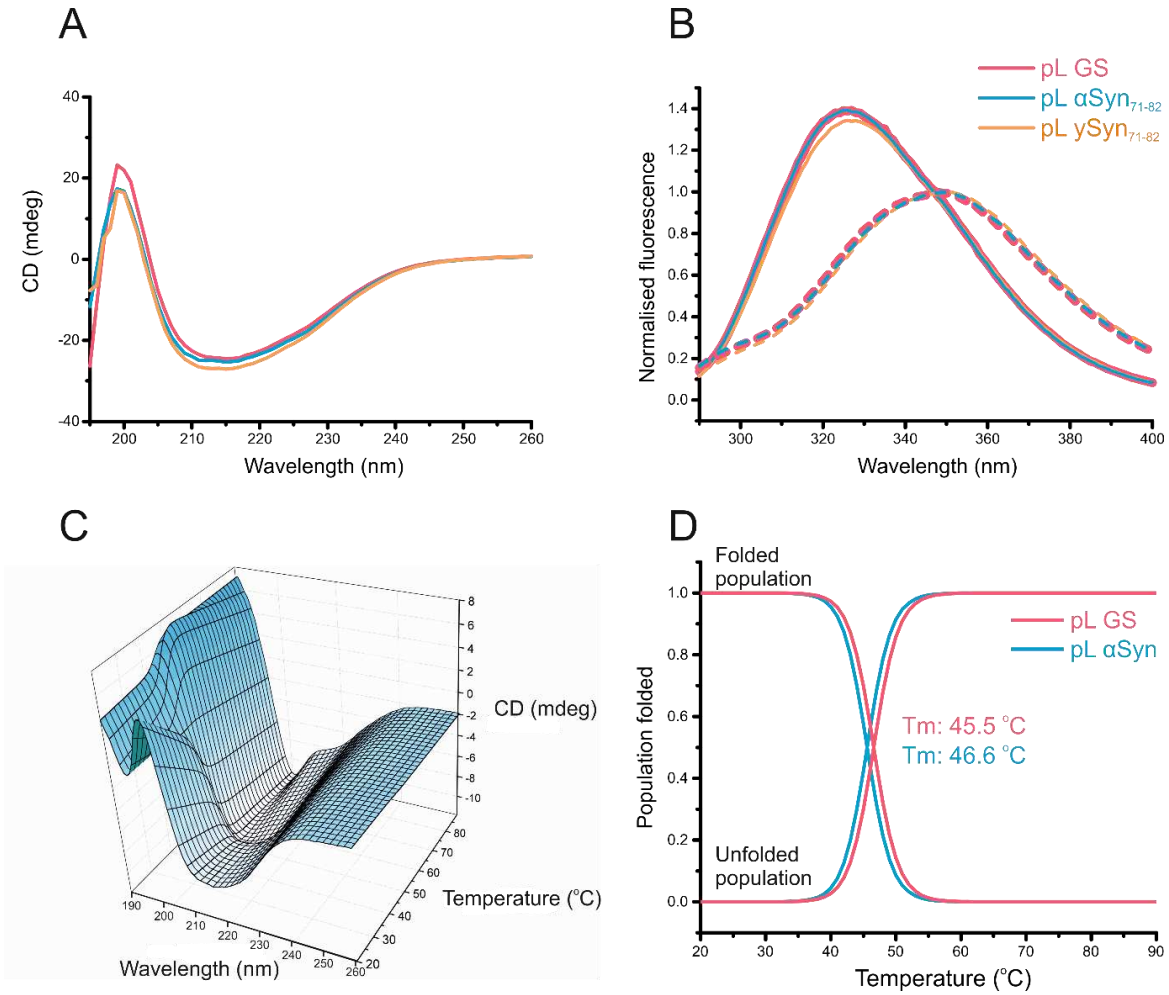

Figure S4. Spectroscopic analyses of pL variants.

(A) Far-UV CD spectra of 50 µM pL GS (pink); pL αSyn_{71-82} (blue) and pL γSyn_{71-82} (orange). The spectra are similar, exhibiting broad minima from ~210-220 nm, consistent with the mixed α/β topology of folded pL. (B) Intrinsic tryptophan fluorescence emission spectra of pL GS (pink), pL αSyn_{71-82} (blue) and pL γSyn_{71-82}, (orange) in the absence (solid lines) or presence of 8M urea (dashed lines). (C) Far UV-CD spectra as a function of temperature for pL αSyn_{71-82}. (D) The relative populations of folded and unfolded conformations of pL αSyn_{71-82} and pL GS (blue and pink respectively) calculated from the global analysis of CD thermal melt data. The T_m values are shown inset.

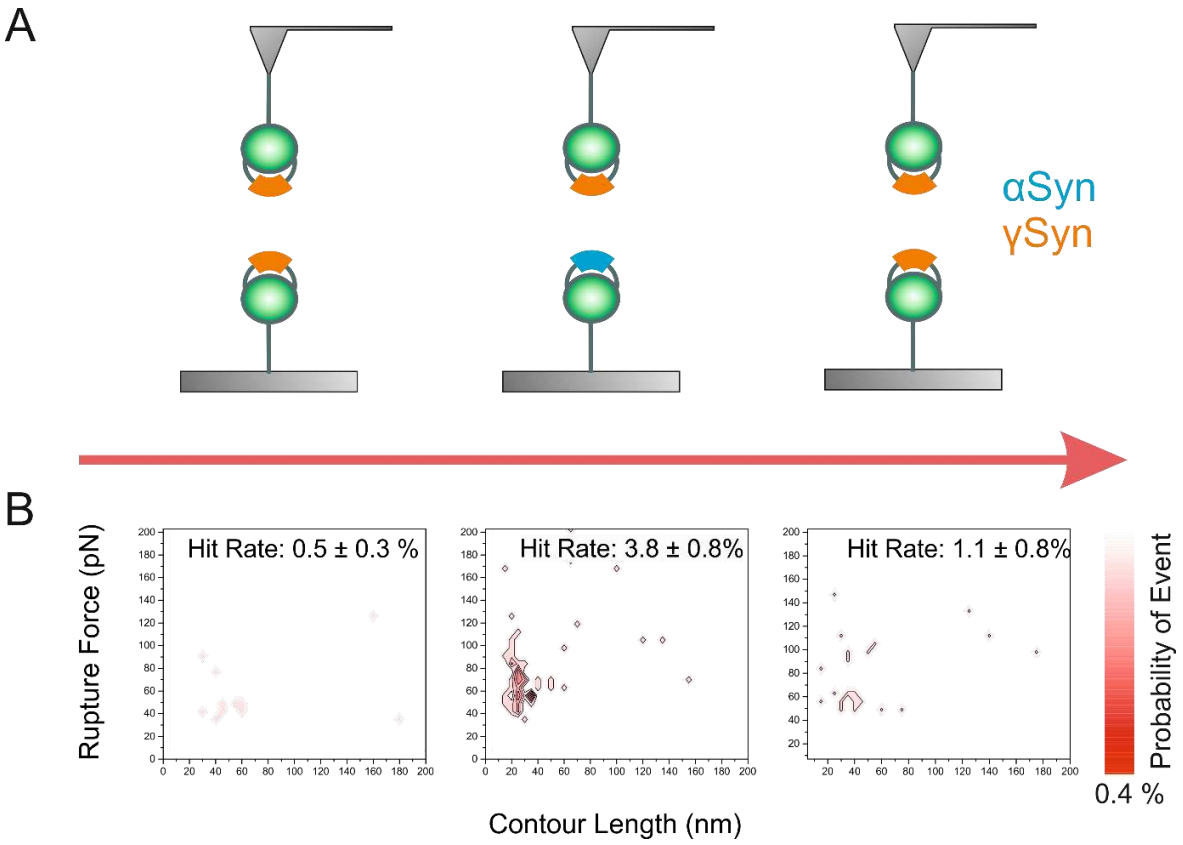

Figure S5. SMFS experiment showing presence of interaction-competent pL γSyn$_{71-82}$ on the AFM tip.

(A) Schematic of experimental setup. First the frequency of dissociation of pL γSyn$_{71-82}$ dimers (hit rate) was measured. The surface was then changed to one derivatised with pL αSyn$_{71-82}$ and the frequency of heterodimer dissociation measured. This sample was then replaced by the original pL γSyn$_{71-82}$ functionalised surface and the dissociation frequency measured once more. (B) Contour plots and calculated hit rates from the experiments described in (A). The intra-experimental errors between force maps are shown. The total number of approach retract cycles was 1500 for each different tip and surface pair.

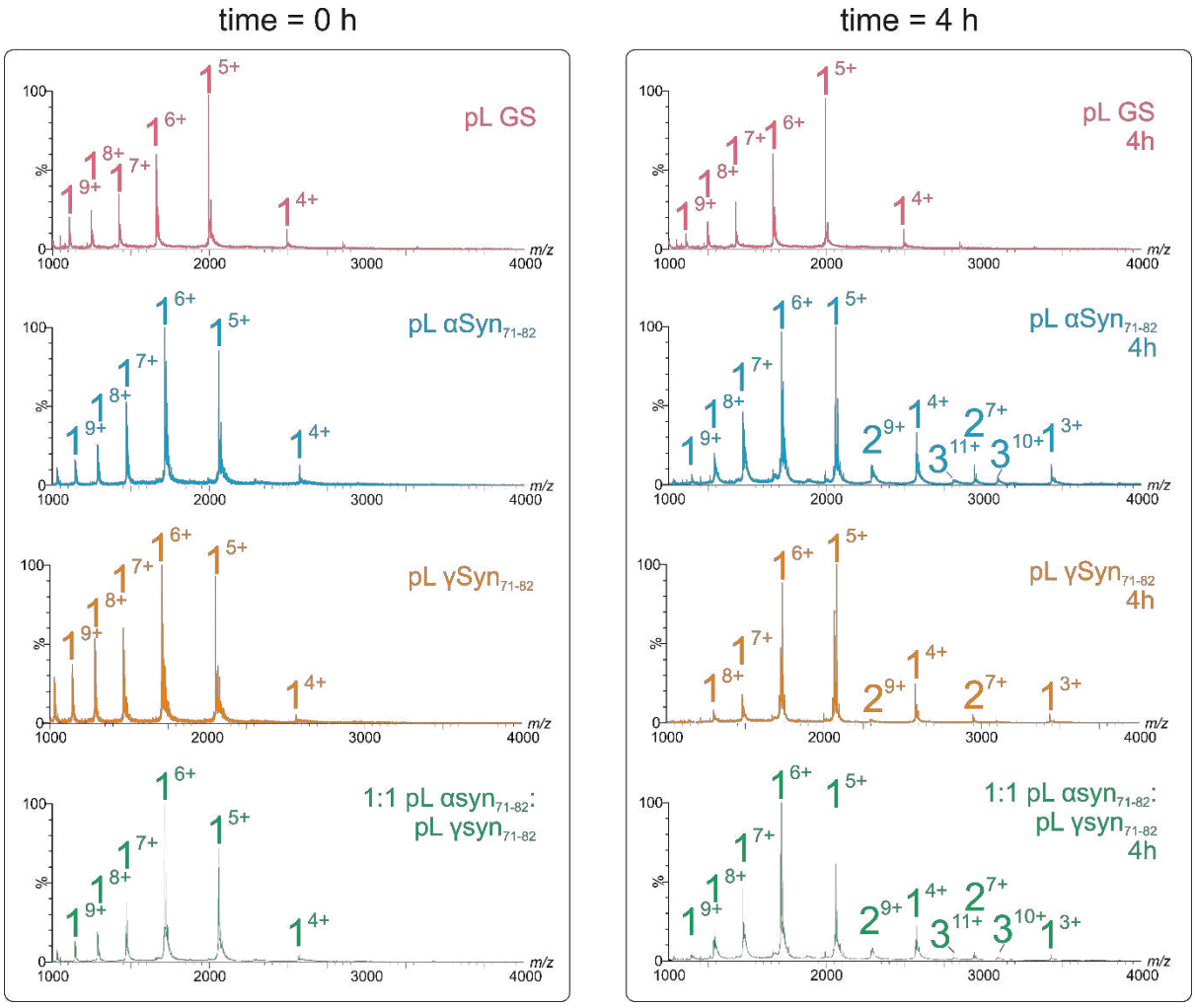

Figure S6. Native ESI-mass spectra of pL constructs immediately after dilution (t = 0) and after 4 h.

ESI-mass spectra of pL GS (pink), pL αSyn_{71-82} (blue), pL γSyn_{71-82} (orange) and a 1:1 mix of pL αSyn_{71-82} and pL γSyn_{71-82} (green) at t= 0 (left) and t = 4 h (right). The numbers above the peaks denote the oligomer order, with the positive-charge state of ions in superscript. All variants in isolation and a 1:1 mixture of pL αSyn_{71-82} and pL γSyn_{71-82} were present as monomer at t = 0 (left panel). After 4 h, all variants except the non-aggregating pL GS construct showed self-association (right panel). All samples were diluted to a final total protein concentration of 100 µM in 100 mM ammonium acetate buffer, pH 6.8.

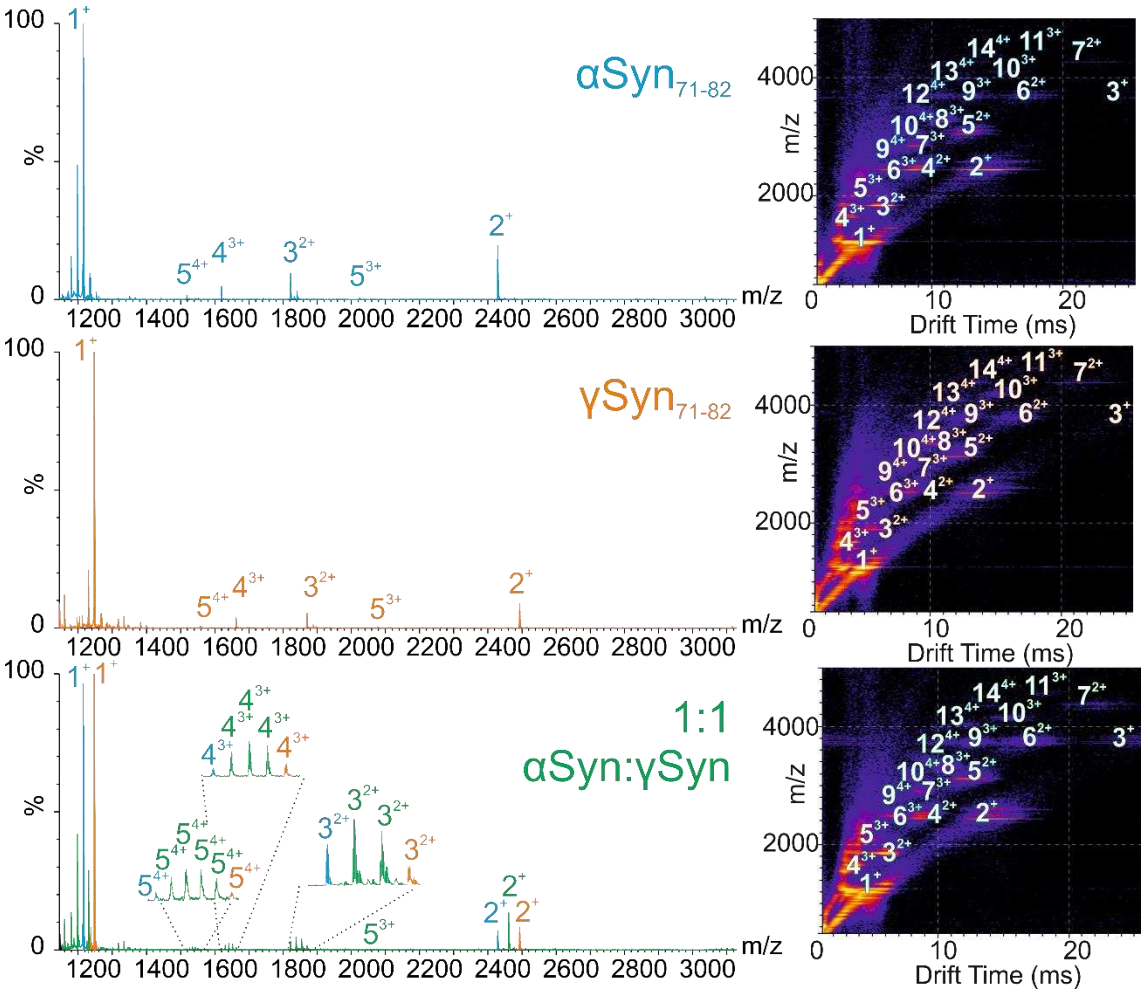

Figure S7. Mass spectrometric analyses of αSyn$_{71-82}$ and γSyn$_{71-82}$ peptides.

ESI mass spectra (left) and ESI IMS-MS driftscope plots (right) of αSyn$_{71-82}$ (top), γSyn$_{71-82}$ (middle) and a 1:1 mix of αSyn$_{71-82}$ and γSyn$_{71-82}$ (bottom). The numbers above the peaks denote the oligomer order, with the positive-charge state of ions in superscript. All mass spectra (left) confirm self-association of the peptides up to pentamer, with the 1:1 mix showing a random distribution between the number of αSyn$_{71-82}$ and γSyn$_{71-82}$ monomers in the oligomers. ESI–IMS–MS Driftscope plots (right) show monomeric to tetradecameric species present in all of the samples, two minutes after diluting the monomer to a final peptide concentration of 100 µM in 100 mM acetate buffer pH 6.8. ESI–IMS–MS Driftscope plots show the IMS drift time versus mass/charge (m/z) versus intensity (z, square-root scale).

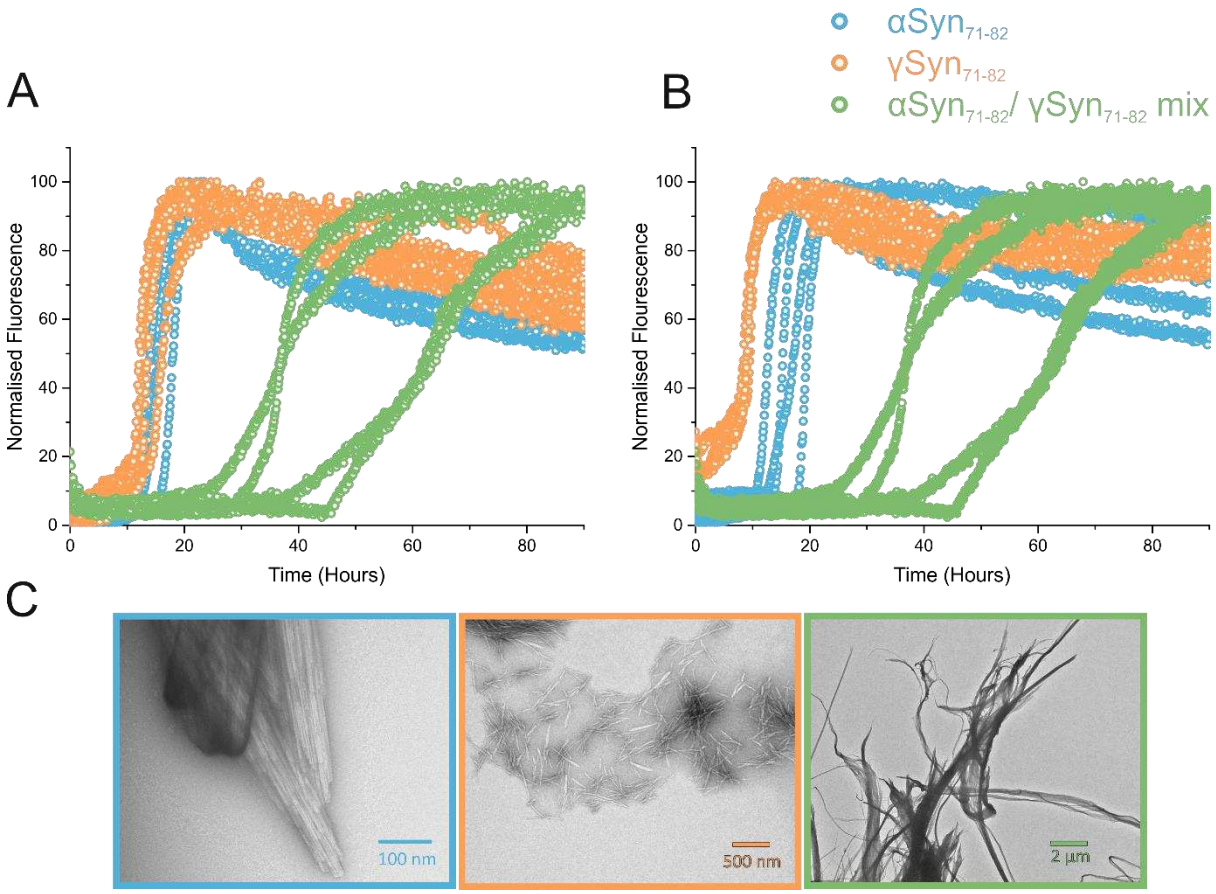

Figure S8. ThT fluorescence assay of αSyn_{71-82} and γSyn_{71-82} synthetic peptides. (A) Normalised fluorescence signal over time of 225 µM αSyn_{71-82} (blue), 225 µM γSyn_{71-82} (orange) and the 1:1 mix of αSyn_{71-82} and γSyn_{71-82} peptides (both at 225 µM, green). The lag times for αSyn_{71-82}, γSyn_{71-82} and for the αSyn_{71-82}:γSyn_{71-82} mixed incubation are 13.2 ± 2.1, 11.8 ± 1.2 and 34.6 ± 8.5 h, respectively. (B) Normalised fluorescence signal over time of 450 µM αSyn_{71-82}, 450 µM γSyn_{71-82} and the 1:1 mix of αSyn_{71-82} and γSyn_{71-82} peptides (both at 225 µM giving a final peptide concentration of 450 µM). Colours denote the same peptides as described in (A). Note: the αSyn_{71-82} + γSyn_{71-82} mix is the same data as presented in (A). The lag times for αSyn_{71-82} and γSyn_{71-82} are 13.3 ± 3.2 and 6.1 ± 1.0 h, respectively. (C) TEM images taken at the end points (100 h) of the incubations (colour coded as above). All three incubations form fibrillary structures, but with notably different morphology.

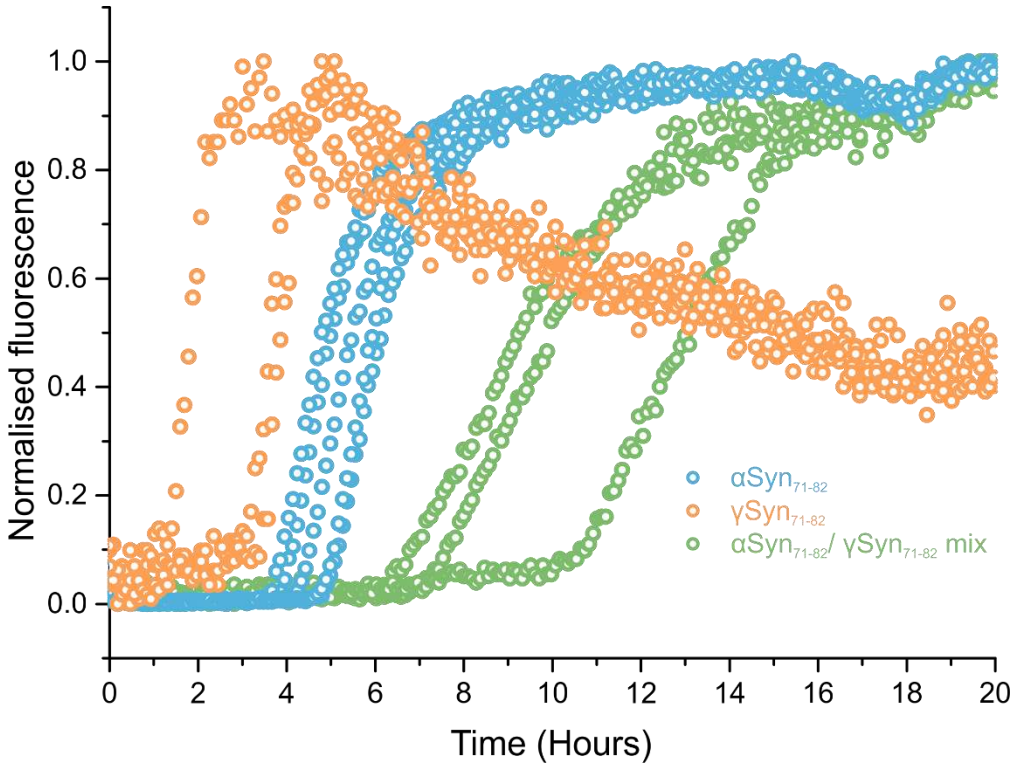

Figure S9. ThT fluorescence assay of αSyn_{71-82} and γSyn_{71-82} synthetic peptides in ESI-MS buffer conditions. Normalised fluorescence signal over time of 225 µM αSyn_{71-82} (blue), 225 µM γSyn_{71-82} (orange) and the 1:1 mix of αSyn_{71-82} and γSyn_{71-82} peptides with a total peptide concentration of 225 µM (both at 112 µM, green). The lag times for αSyn_{71-82}, γSyn_{71-82} and for the αSyn_{71-82}:γSyn_{71-82} mixed incubation are 4.2 ± 0.6, 2.5 ± 1.1 and 7.8 ± 2.0 h, respectively. ThT experiments presented here were carried out in 100 mM ammonium acetate, pH 6.8 (in line with the ESI-MS experimental conditions).

Supplementary Tables

Protein	Expected mass Da	Observed mass Da	Mass difference (Da)
pL GS	10 100	9 967 ± 3	-133
pL αSyn_{71-82}	10 390	10 257 ± 4	-132
pL γSyn_{71-82}	10 423	10 290 ± 4	-133

Supplementary Table 1. Observed and expected masses from ESI-MS data. The observed mass is 133 Da below the expected mass as the N-terminal Met residue is excised, due to the activity of the *E. coli* enzyme methionyl-aminopeptidase which has increased activity with decreasing residue size in the penultimate N-terminal position (alanine in this case)(1). Errors are quoted to the nearest Dalton.

References

1. Hirel PH, Schmitter JM, Dessen P, Fayat G, Blanquet S (1989) Extent of N-terminal methionine excision from *Escherichia coli* proteins is governed by the side-chain length of the penultimate amino-acid. *Proc Natl Acad Sci USA* **86**:8247-8251.